PasT of Escherichia coli sustains antibiotic tolerance and aerobic respiration as a bacterial homolog of mitochondrial Coq10

Cinzia Fino, Martin Vestergaard, Hanne Ingmer, Fabien Pierrel, Kenn Gerdes, Alexander Harms

Received: 3 March 2020 | Revised: 24 April 2020 | Accepted: 11 May 2020

DOI: 10.1002/mbo3.1064

ORIGINAL ARTICLE

MicrobiologyOpen Open Access WILEY

PasT of *Escherichia coli* sustains antibiotic tolerance and aerobic respiration as a bacterial homolog of mitochondrial Coq10

Cinzia Fino[1] | Martin Vestergaard[2] | Hanne Ingmer[1,2] | Fabien Pierrel[3] | Kenn Gerdes[1] | Alexander Harms[1,4]

[1]Department of Biology, Centre for Bacterial Stress Response and Persistence, University of Copenhagen, Copenhagen, Denmark

[2]Department of Veterinary and Animal Sciences, Faculty of Health and Medical Sciences, University of Copenhagen, Frederiksberg, Denmark

[3]CNRS, Grenoble INP, TIMC-IMAG, Université Grenoble Alpes, Grenoble, France

[4]Focal Area of Infection Biology, Biozentrum, University of Basel, Basel, Switzerland

Correspondence
Kenn Gerdes and Alexander Harms, Department of Biology, Centre for Bacterial Stress Response and Persistence, University of Copenhagen, Copenhagen, Denmark.
Emails: kenn.gerdes5@gmail.com (KG); alexander.harms@unibas.ch (AH)

Funding information
Novo Nordisk Fonden; Danmarks Grundforskningsfond, Grant/Award Number: DNRF120; Schweizerischer Nationalfonds zur Förderung der Wissenschaftlichen Forschung, Grant/Award Number: Ambizione PZ00P3_180085; European Molecular Biology Organization, Grant/Award Number: ALTF 564-2016

Abstract

Antibiotic-tolerant persisters are often implicated in treatment failure of chronic and relapsing bacterial infections, but the underlying molecular mechanisms have remained elusive. Controversies revolve around the relative contribution of specific genetic switches called toxin–antitoxin (TA) modules and global modulation of cellular core functions such as slow growth. Previous studies on uropathogenic *Escherichia coli* observed impaired persister formation for mutants lacking the *pasTI* locus that had been proposed to encode a TA module. Here, we show that *pasTI* is not a TA module and that the supposed toxin PasT is instead the bacterial homolog of mitochondrial protein Coq10 that enables the functionality of the respiratory electron carrier ubiquinone as a "lipid chaperone." Consistently, *pasTI* mutants show pleiotropic phenotypes linked to defective electron transport such as decreased membrane potential and increased sensitivity to oxidative stress. We link impaired persister formation of *pasTI* mutants to a global distortion of cellular stress responses due to defective respiration. Remarkably, the ectopic expression of human *coq10* largely complements the respiratory defects and decreased persister levels of *pasTI* mutants. Our work suggests that PasT/Coq10 has a central role in respiratory electron transport that is conserved from bacteria to humans and sustains bacterial tolerance to antibiotics.

KEYWORDS
antibiotic tolerance, electron transport chain, persistence, toxin–antitoxin, ubiquinone, uropathogenic *Escherichia coli*

1 | INTRODUCTION

Bacterial persisters are cells that transiently display antibiotic tolerance due to a dormant physiology and constitute a subpopulation of cells within the overall bacterial population (Balaban et al., 2019). This phenomenon has been linked to treatment failure of chronic and relapsing infections in different clinical settings (Fauvart, De Groote, & Michiels, 2011; Harms, Maisonneuve, & Gerdes, 2016; Lewis, 2010). One common example is urinary tract infections (UTIs) that often relapse and are frequently caused by uropathogenic strains of *Escherichia coli* (UPEC) (Flores-Mireles, Walker, Caparon, & Hultgren, 2015). These bacteria are thought

Kenn Gerdes and Alexander Harms should be considered joint senior authors.

to persist during antibiotic treatment in rectal reservoirs and intracellular biofilms, and the survival of UPECs isolated from recurrent UTIs was shown to correlate with higher levels of persister cells detectable in the population (Anderson et al., 2003; Blango & Mulvey, 2010; Glover, Moreira, Sperandio, & Zimmern, 2014; Goneau et al., 2014).

Although persister cells are ubiquitous and their formation and evolution have been studied in multiple human pathogens (Michiels, Van den Bergh, Verstraeten, Fauvart, & Michiels, 2016), the molecular mechanisms underlying their antibiotic tolerance have remained largely elusive. Mechanistic studies have been performed primarily in laboratory model strains like *E. coli* K-12 where multiple different pathways of persister cell formation have been described (Harms et al., 2016; Lewis, 2010). Among these, the dormant physiology of persister cells has been linked repeatedly to the reversible activation of toxin–antitoxin (TA) systems in different strains of *E. coli* as well as closely related *Salmonella* Typhimurium (Dörr, Vulic, & Lewis, 2010; Harms et al., 2016; Helaine et al., 2014; Norton & Mulvey, 2012; Verstraeten et al., 2015). TA systems are composed of a toxin protein that can inhibit key cellular processes and a cognate antitoxin that represses the toxin's activity until it is degraded in response to cellular signaling (Harms, Brodersen, Mitarai, & Gerdes, 2018). They can therefore act as genetically controlled switches to reversibly shut down bacterial growth, and as such, it is generally intuitive that TA systems might be well suited to control persister cell formation, survival, and resuscitation (Ronneau & Helaine, 2019). However, the relative importance of specific factors such as TA systems has remained controversial compared to global changes via modulation of the cellular core machinery including electron transport or ATP synthesis (Goneau et al., 2014; Goormaghtigh et al., 2018; Harms et al., 2016; Pontes & Groisman, 2019; Shan et al., 2017). We previously discovered that a once well-established link between ten particular TA systems of *E. coli* K-12 and persister formation is wrong (Goormaghtigh et al., 2018; Harms, Fino, Sørensen, Semsey, & Gerdes, 2017), and the link between TA systems and persister formation in *Salmonella* Typhimurium has also recently been disputed (Pontes & Groisman, 2019).

Given these debates, we became interested in a study that found the *pasTI* TA module of UPEC strain CFT073 to be critical for antibiotic-tolerant persister cells (Norton & Mulvey, 2012). Remarkably, the orthologous system in *E. coli* K-12, *ratAB*, seemed to play no role in persister formation under the same conditions. However, the molecular basis of PasTI-dependent drug tolerance in UPECs remained unclear. Previous work had proposed that the RatA toxin of *E. coli* K-12 is a translation inhibitor that interferes with 70S ribosome assembly but did not experimentally confirm the role of RatB as the cognate antitoxin, questioning the notion that RatAB/PasTI is indeed a TA system (Zhang & Inouye, 2011).

In this study, we therefore aimed at uncovering the molecular activity and biological function of PasTI/RatAB in *E. coli* to shed more light on the role of this TA system in persister formation and persister cells in clinical contexts. While we readily reproduced that PasT is critical for the formation or survival of ciprofloxacin-tolerant cells by *E. coli* CFT073 and other pathogenic enterobacteria, we could not confirm that PasTI is a TA system. Instead, we show that PasT is the bacterial homolog of mitochondrial protein Coq10 that acts as an important accessory factor in the ubiquinone-dependent electron transport chain (ETC). We find that *E. coli* mutants lacking *pasT* display the same pleiotropic phenotypes as yeast *coq10* mutants including decreased membrane potential, increased sensitivity to oxidative stress, and modestly decreased ubiquinone biosynthesis. Remarkably, these signs of defective respiration in *E. coli* can be complemented by ectopic expression of human *coq10*, suggesting that PasT and Coq10 are functionally equivalent. We therefore conclude that PasT is a previously unrecognized player in bacterial respiratory electron transport and likely affects antibiotic tolerance indirectly via its roles in redox balance and/or energy metabolism.

2 | MATERIALS AND METHODS

2.1 | Bacterial handling and culturing

Escherichia coli was routinely cultured in LB or M9 liquid medium at 37°C in glass culture tubes or Erlenmeyer flasks with agitation at 160 rpm, usually in a water bath shaker for physiological experiments. LB agar plates were routinely used as a solid medium. Selection for plasmid maintenance was performed with ampicillin at 30 μg/ml (mini-R1 origin of replication) or 100 μg/ml (other origins of replication), chloramphenicol at 25 μg/ml, and kanamycin at 25 μg/ml. P*lac* was induced with 1 mM of isopropyl β-D-1-thiogalactopyranoside (IPTG), while P*araB* was induced with 0.2% w/v of L-arabinose. Whenever appropriate, liquid and solid media were supplemented with 1% w/v D-glucose to reduce basal expression of both P*lac* and P*araB* promoters through catabolite repression. Unless indicated differently, the complementation of bacterial mutants with *E. coli* genes was performed using low-copy plasmids (pNDM220 derivatives) carrying these genes including their own promoter, so that no ectopic induction of the constructs was necessary. When enforced expression was required (e.g., for the experiments shown in Figure 1 and Figure A6f in Appendix 2) or to test heterologous complementation with distant homologs (e.g., Figure 8), isogenic plasmids encoding genes without their endogenous promoters were used and the bacteria were continuously cultured in the presence of 1 mM of IPTG in overnight cultures and throughout the experiment to induce expression from the P*lac* promoter of pNDM220 derivatives (see all plasmids listed in Table A2 in Appendix 1).

Bacteria were grown anaerobically on LB agar plates incubated in a plastic jar (cat# 1.16387.0001; Merck) with an anaerobic atmosphere generation bag (cat# 68061; Sigma). The formation of an anaerobic atmosphere was confirmed using Anaerotest strips (cat# 1.15112.0001; Merck). 1% w/v D-glucose was added as a fermentable carbon source to LB agar plates incubated anaerobically.

2.2 | Preparation of culture media

Lysogeny broth (LB) was prepared by dissolving 1% w/v of tryptone (cat# LP0042; Oxoid), 0.5% w/v of yeast extract (cat# LP0021; Oxoid), and 1% w/v of sodium chloride (cat# 27810.364; VWR Chemicals) in Milli-Q H_2O and sterilized by autoclaving. LB agar plates were prepared by supplementing LB medium with agar and 1.5% w/v before autoclaving. M9 medium was prepared according to the Cold Spring Harbor Protocols (M9 minimal medium (standard), 2010) with modifications in the form of 1× M9 salts (stock solution prepared from 5× M9 salts, see below) supplemented with 0.4% w/v Amicase (cat# 1002372245; Sigma; from 10% w/v sterile-filtered stock), 0.4% w/v D-glucose (cat# 101176K; VWR Chemicals; from 40% w/v autoclaved stock), 2 mM $MgSO_4$ (cat#. 25.165.292; VWR Chemicals), 1 µg/ml thiamine (cat# T1270; Sigma), and 100 µM $CaCl_2$ (cat# C3306; Sigma). The 5× M9 salt solution was prepared by dissolving 25.6 g Na_2HPO_4 (cat# S9390; Merck), 6 g KH_2PO_4 (cat# P0662; Sigma), 1 g NaCl (cat# 277810.364; VWR Chemicals), and 2 g NH_4Cl (cat# 5470.1; Roth) in 400 ml Milli-Q H_2O supplemented with 20 µl of a 10 mg/ml $FeSO_4$ solution (cat# F8048; Sigma). After confirming a pH of 7.4, the solution was sterile-filtered and stored in the dark.

2.3 | Strain construction

E. coli K-12 MG1655 Δ*ratAB* and *E. coli* CFT073 Δ*pasTI* mutants (with identifiers CF083 and CF069/CF378, respectively) were constructed as scarless deletions using two-step recombineering with a double-selectable cassette encoding chloramphenicol resistance and *sacB* (sucrose sensitivity) that was amplified from template plasmid pKO4 (Lee et al., 2001). Recombineering functions were expressed from pWRG99 (Blank, Hensel, & Gerlach, 2011). The first step of recombineering replaced the target gene with the double-selectable cassette, and the second step removed the double-selectable cassette via recombineering with a pair of annealed 80-mer oligonucleotides composed of twice 40 bp homologies flanking the desired deletion (Blank et al., 2011). The negative selection was performed on LB agar plates supplemented with 6% w/v sucrose (cat# S0389; Sigma; from a 60% w/v sterile-filtered stock solution). *E. coli* K-12 MG1655 and *E. coli* CFT073 derivatives were routinely transformed with plasmids using TSS transformation (Chung, Niemela, & Miller, 1989) and electroporation, respectively. Deletions of *pasTI* in *E. coli* strains O157:H7 EDL933 and 55989 as well as in *Salmonella enterica* subsp. *enterica* Typhimurium strain SR-11 were constructed using recombineering functions expressed from pKM208 of Murphy and Campellone (2003). For *E. coli* EDL933 and *S. enterica* SR-11, scarless deletions via the double-selectable cassette of pWRG100 were achieved (see above). For *E. coli* 55989, the *pasTI* locus was first replaced with an FRT-flanked gene cassette encoding kanamycin resistance. In the second step, gene cassettes were removed using Flp recombinase expressed from pCP20 in a way that only a short FRT scar remained. All bacterial strains used in this study are listed in Table A1 (Appendix 1), all plasmids are listed in Table A2 (Appendix 1), and all oligonucleotides are listed in Table A3 (Appendix 1).

2.4 | Plasmid construction

Plasmids were constructed using standard techniques of restriction-based molecular cloning. Briefly, a PCR-amplified fragment and the vector backbone were each cut with appropriate FastDigest restriction enzymes (Thermo Scientific). After fragment purification and backbone dephosphorylation (using FastAP dephosphorylase; Thermo Scientific), the two components were ligated together using the T4 ligase (Thermo Scientific). Site-directed mutagenesis of plasmids was performed by PCR with partially overlapping primers as described by Liu and Naismith (2008). Plasmid construction was always confirmed by DNA sequencing. A list of all plasmids used in this study as well as details of their construction are given in Table A2 (Appendix 1). The sequences of all oligonucleotides used in this study are listed in Table A3 (Appendix 1).

The open reading frames of *Caulobacter crescentus cc1736* and human *coq10A* (one of the two human *coq10* isoforms) were obtained from GenScript after codon optimization for heterologous expression in *E. coli*. For *coq10*, we cloned the C-terminal portion homologous to *pasT*/*cc1736* without the N-terminal mitochondrial signal peptide sequence at its 5′ end (see Figure A4a in Appendix 2).

2.5 | Sequence analyses and in silico predictions

For the protein alignment shown in Figure A4a of Appendix 2, amino acid sequences of *E. coli* CFT073 PasT (UniProt accession Q8FEY4), *C. crescentus* CC1736 (UniProt accession Q9A7I7), Coq10 of *Schizosaccharomyces pombe* (UniProt accession Q9USM9), and *Saccharomyces cerevisiae* (UniProt accession Q08058), as well as human Coq10A (UniProt accession Q96MF6), were aligned using MAFFT (implemented in Geneious v10.1.3) and manually curated. For the synteny analysis of *pasTI* loci shown in Figure 3, the presence of prophages at a known integration hotspot next to *ssrA* (see Mao et al. (2009)) was detected with PHASTER (Arndt et al., 2016) while the integration of other specific gene content was analyzed by manual sequence comparisons.

Phyre2 (https://www.sbg.bio.ic.ac.uk/phyre2; Kelley, Mezulis, Yates, Wass, & Sternberg, 2015) was used for the prediction of the tertiary structure of PasT (Figure A4b in Appendix 2). The prediction of potential functional partners in Figure A4c in Appendix 2 was obtained using STRING (https://string-db.org/; Szklarczyk et al., 2018).

2.6 | Spot assays

For the detection of bacterial growth inhibition upon expression of different proteins, 1.5 ml of dense overnight cultures of *E. coli* harboring indicated plasmids was adjusted to have the same optical

density at 600 nm (OD600), washed once, and then serially diluted in sterile phosphate-buffered saline (PBS). Subsequently, 10 µl of the serial dilutions was spotted on LB agar plates containing indicated supplements that induce or repress protein expression. Different copy numbers of otherwise isogenic plasmid vectors were achieved by merely changing the origin of replication on the otherwise identical plasmid backbone. Based on pNDM220 (mini-R1 origin, low-copy; Gotfredsen & Gerdes, 1998), we thus created pAH186_SC101 and pAH186_ColE1 with SC101 (medium-copy) and ColE1 (high-copy) origins, respectively (Jahn, Vorpahl, Hubschmann, Harms, & Muller, 2016). We assume that *pasT/ratA* cloned in pNDM220 is expressed at physiologically relevant levels due to a low plasmid copy number that should drive expression similar to the native chromosomal loci. A recent proteomic study revealed that RatA(YfjG) and RatB(YfjF) are expressed, under conditions identical to our experimental conditions (M9 medium with glucose as sole carbon source), to levels of ca. 30 and 50 molecules per cell, respectively (Supplementary Table 9 in Schmidt et al. (2015)).

The Doc and HipA TA system toxins are kinases that inhibit bacterial growth through phosphorylation and concomitant inactivation of elongation factor Tu (EF-Tu) or glutamyl tRNA synthetase, respectively (Castro-Roa et al., 2013; Germain, Castro-Roa, Zenkin, & Gerdes, 2013). To compare the colony size between strains, 1.5 ml of dense overnight cultures was washed in 100 µl of phosphate-buffered saline (PBS), serially diluted in PBS, and spotted (10 µl) on LB agar plates. When indicated, LB agar plates were supplemented with inducers and/or incubated under anaerobic conditions.

2.7 | Determination of minimum inhibitory concentration (MIC)

The MIC of antibiotics for different *E. coli* strains was determined by broth dilution assays. In short, serial 1.5-fold dilutions of antibiotics in M9 medium with suitable supplements were inoculated with the different bacterial strains as indicated, sealed with a breathable film, and agitated at 37°C/160 rpm overnight. The MIC was determined as the lowest concentration of antibiotic that prevented bacterial growth as detected by visual inspection.

2.8 | Antibiotic tolerance assays

The dynamics of antibiotic tolerance throughout the growth phases of *E. coli* were studied by performing antibiotic killing assays with bacterial cultures that had grown for different times after inoculation from overnight culture into the fresh medium as described previously (Harms et al., 2017). In more detail, overnight cultures were inoculated from single colonies into 3 ml of M9 medium and grown for ca. 16 hr in plastic culture tubes (cat# 62.515.006; Sarstedt). Subcultures of 10 ml M9 medium in Erlenmeyer flasks were inoculated 1:100 from these overnight cultures and agitated in a water bath at 37°C/160 rpm. All viable colony-forming units (cfu) and antibiotic-tolerant cfu (see below) were determined for isogenic cultures that had grown for different times after subculturing (from 0 hr to 8 hr) and represented the spectrum of bacterial growth phases from lag phase over exponential growth into stationary phase (see, e.g., the curve of colony-forming units (cfu) plotted over time in Figure 2a). Antibiotic tolerance was assayed by treating 3 ml aliquots of culture in plastic tubes with lethal concentrations of ciprofloxacin (10 µg/ml), ampicillin (100 µg/ml), or colistin (6.6 µg/ml) for 5 hr at 37°C/160 rpm. In parallel, cfu counts of the same untreated cultures were determined by plating serial dilutions on LB agar plates. The MIC of ciprofloxacin for *E. coli* K-12 MG1655 and CFT073 including all tested mutant derivatives was 0.00780 µg/ml, that is, the bacteria were treated with >1,000× MIC to avoid secondary effects of prophage activation (Harms et al., 2017). The MIC of colistin for *E. coli* K-12 MG1655 and CFT073 including all tested mutant derivatives was 1.3 µg/ml, that is, the treatment was done with ca. 4× MIC. The MIC of ampicillin was found to be 8.88 µg/ml for the K-12 strains and 33 µg/m for the CFT073 strains, meaning that treatment with 100 µg/ml ampicillin (following reference Norton & Mulvey, 2012) represented 11× MIC and 3× MIC, respectively.

After antibiotic treatment, 1.5 ml of the samples was washed in 1 ml of PBS, concentrated in 100 µl of PBS, serially diluted in PBS, and spotted (10 µl) on LB agar plates. Agar plates were incubated at 37°C for at least 24 hr, and cfu counts per milliliter were determined from spots containing 10 to 100 bacterial colonies. The fraction of antibiotic-tolerant cells was calculated as the ratio of the cfu counts per milliliter after and before antibiotic treatment. To verify that antibiotic-tolerant cfu represented persister cells, we performed time–kill curves and confirmed biphasic kinetics of antibiotic killing (see, e.g., Figure A2a in Appendix 2).

2.9 | Hydrogen peroxide sensitivity assay

The dynamics of hydrogen peroxide sensitivity throughout bacterial growth phases were assayed similarly to the antibiotic tolerance assay with the exception that bacteria were challenged with 10 mM of hydrogen peroxide (H_2O_2) (from 10 M stock; #cat 31642; Sigma) for 30 min instead of antibiotic treatment. Furthermore, experiments were only performed with bacteria grown up to no later than late-exponential phase (4 hr after inoculation 1:100 from overnight culture) because we consistently observed complete tolerance to H_2O_2 in the stationary phase for all bacterial strains. When indicated, the cultures were treated with 20 mM of the antioxidant ascorbate (vitamin C; from 1 M stock; cat# A5960) for 20 min before the challenge with H_2O_2.

2.10 | Assessment of membrane potential using $DiOC_2(3)$

The bacterial membrane potential was assessed using indicator dye 3,3′-diethyloxacarbocyanine iodide ($DiOC_2(3)$) as implemented in

the *Bac*Light Bacterial Membrane Potential Kit (Invitrogen, Thermo Fischer Scientific) according to the manufacturer's recommendations. The $DiOC_2(3)$ dye shows green fluorescence in bacteria at low concentrations but becomes more concentrated in cells with larger membrane potential, causing it to aggregate and shift the fluorescence toward red emission.

Per strain and replicate, 2 µl cells from stationary-phase cultures were inoculated into 2 ml of fresh LB medium in 14-ml Falcon round-bottom tubes (Corning) and grown to an OD_{600} of 0.2 at 37°C with shaking (180 rpm). 10 µl culture was transferred to 980 µl filtered phosphate-buffered saline. To each cell solution, 10 µl of a 3 mM $DiOC_2(3)$ solution was added and cells were stained for 30 min at room temperature. The assay was verified by depolarizing the membrane with the protonophore carbonyl cyanide 3-chlorophenylhydrazone (CCCP) at a final concentration of 5 µM. Data were recorded on a BD Biosciences Accuri C6 Flow Cytometer (Becton, Dickinson, and Company), with emission filters suitable for detecting red and green fluorescence. Settings on the flow cytometer were as follows: 25'000 recorded events at an FSC threshold of 15.000 and medium flow rate. Gating of stained cell population and analysis of flow cytometry data were performed in CFlow® (BD Accuri). As an indicator of membrane potential, the ratio of red to green fluorescence intensity was calculated.

2.11 | Quantification of ubiquinone biosynthesis and levels

Levels of isoprenoid quinones were determined in cell extracts using HPLC-ECD-MS (electrochemical detection–mass spectrometry) as previously described (Hajj Chehade et al., 2019; Loiseau et al., 2017). The de novo synthesis of ubiquinone (UQ_8) and its early biosynthetic intermediate octaprenyl-phenol (OPP) was studied by supplementing bacterial cultures with their ^{13}C-labeled precursor 4-hydroxybenzoic acid (4-HB) and analyzing the accumulation of ^{13}C label in the molecules of interest. An illustration of the UQ_8 biosynthetic pathway in *E. coli* was included in Figure 5a for clarity.

Bacterial subcultures in 10 ml of M9 medium in Erlenmeyer flasks were inoculated 1:100 from dense overnight cultures and agitated in a shaking water bath at 37°C/160 rpm to early log phase (2 hr of growth for wild-type and Δ*pasTI*/Δ*ratAB* strains; ca. 10^8 cfu/ml) or late log phase (4 hr of growth for wild-type and Δ*pasTI*/Δ*ratAB* strains; ca. 10^9 cfu/ml) and then supplemented with 10 µM $^{13}C_7$-4-HB (cat# 587869; Sigma) for an additional period of 30 min. Subsequently, cells were cooled on ice, harvested by centrifugation, and washed with 1 ml of cold PBS. The weight of each cell pellet was determined, a proportional amount of the UQ_{10} standard was added, and isoprenoid quinones were extracted and analyzed by HPLC-ECD-MS. Single-ion monitoring detected the following molecules: $^{13}C_6$-OPP ($M+NH_4^+$), m/z 662.0–663.0, 5–10 min, scan time 0.2 s; UQ_8 ($M+H^+$), m/z 727.0–728.0, 6–10 min, scan time 0.2 s; $^{13}C_6$-UQ_8 ($M+H^+$), m/z 733.0–734.0, 6–10 min, scan time 0.3 s; and UQ_{10} ($M+NH_4^+$), m/z 880.2–881.2, 10–17 min, scan time 0.2 s. Peak areas were corrected for sample loss during extraction based on the recovery of the UQ_{10} internal standard (typically higher than 80%) and were then normalized to the cell's wet weight. The ECD signal of UQ_8 was converted into picomoles based on a calibration curve obtained with commercial UQ_{10}.

2.12 | Quantification and statistical analysis

Data sets were analyzed by calculating the mean and standard deviation of at least three biological replicates for each experiment. Detailed information for each experiment is provided in the figure legends.

3 | RESULTS

3.1 | *pasTI* does not encode a toxin–antitoxin system

One previous study proposed that the *pasTI* locus encodes a new TA system composed of the PasT toxin and the PasI antitoxin (Norton & Mulvey, 2012). However, we did not detect any growth inhibition of *E. coli* CFT073 when *pasT* was either expressed at physiologically relevant levels from a low-copy-number plasmid or overexpressed from isogenic plasmids replicating at higher copy numbers (Figure 1). Deletion mutants lacking the chromosomally encoded *pasTI* locus, a possible source of experimental interference, also failed to show any inhibition of growth upon *pasT* overexpression (Figure A1a, Appendix 2). Similarly, the expression of *pasT* failed to inhibit the growth of *E. coli* K-12 MG1655 (Figure A1b, Appendix 2). No growth inhibition was also observed upon expression of the proposed antitoxin *pasI* (Figure A1c, Appendix 2). We therefore concluded that the *pasTI* locus is unlikely to encode a TA system.

3.2 | Lack of pasT impairs antibiotic tolerance of *E. coli* CFT073

To gain deeper insight into the role of *pasTI* in *E. coli* persister formation, we monitored the level of antibiotic-tolerant cells throughout the different bacterial growth phases as previously described (Harms et al., 2017). Interestingly, we observed decreased survival of the *E. coli* CFT073 Δ*pasTI* mutant when treated with ciprofloxacin compared to the wild-type during exponential growth and over into the stationary phase. This defect in survival was caused by a lower level of persister cells in the Δ*pasTI* mutant population (Figure 2a; see also Figure A2a in Appendix 2), and similar results were obtained for treatment with the membrane-targeting antibiotic colistin (Figure A2b,d,f in Appendix 2). For the β-lactam ampicillin, we observed increased levels of tolerant cells for the Δ*pasTI* mutant, possibly caused by its partial growth defect since this class of antibiotics only kills actively growing cells (Figure A2c,e in Appendix 2). Conversely, no phenotype was observed at any time of the growth curve when comparing antibiotic tolerance of *E. coli* K-12 MG1655 and its Δ*ratAB* derivative (Figure 2b; see also Figure A2a in Appendix 2).

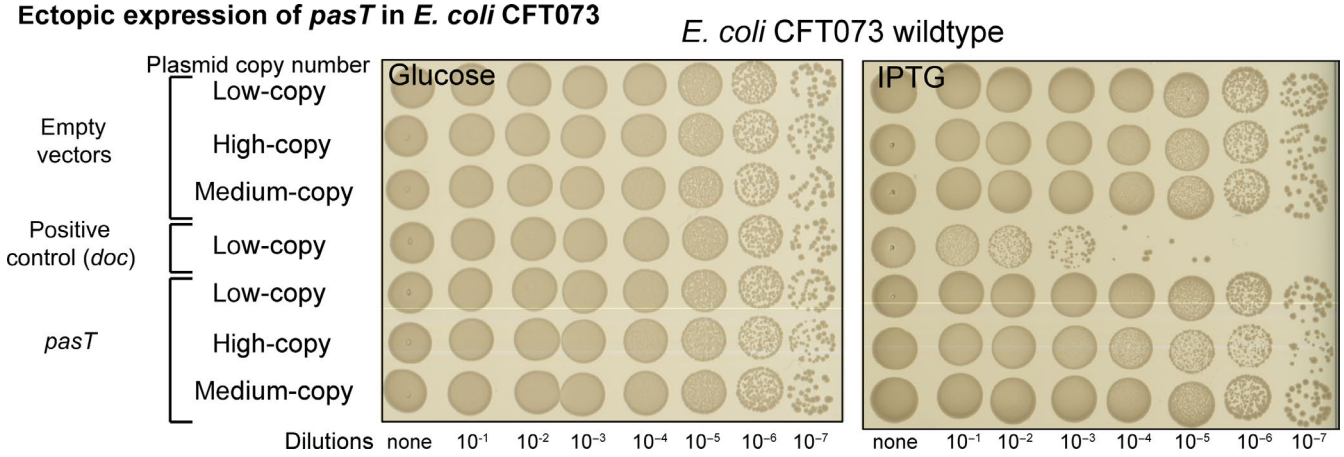

FIGURE 1 PasT does not inhibit bacterial growth. Spot assay of *E. coli* CFT073 harboring isogenic plasmids with different copy number encoding either *pasT* or the well-studied TA module toxin *doc* (as positive control) under the control of a P*lac* promoter on LB agar plates containing 1 mM isopropyl β-D-1-thiogalactopyranoside (IPTG) and repressed on LB agar plates containing 1% w/v D-glucose (see details in Materials and Methods). Similar results were obtained for *pasT* expression in *E. coli* CFT073 Δ*pasTI*, *E. coli* K-12 MG1655, and *E. coli* K-12 MG1655 Δ*ratAB* (Figure A1a/b in Appendix 2). No growth inhibition was also observed for the expression of *pasI* (Figure A1c in Appendix 2).

These results were overall consistent with the previous observation that *pasTI* is somehow critical for the formation or survival of antibiotic-tolerant persister cells in *E. coli* CFT073 but that *ratAB* in *E. coli* K-12 MG1655 is not (Norton & Mulvey, 2012). Both the *pasTI* and *ratAB* loci, provided *in trans* from a low-copy plasmid, as well as *pasT* or *ratA* alone, could complement the phenotype of decreased ciprofloxacin persister levels of *E. coli* CFT073 Δ*pasTI* (Figure 2c,d; see also Figure A2a in Appendix 2). These results demonstrate that the defect of *E. coli* CFT073 Δ*pasTI* in persister formation or survival is linked to the lack of PasT. Furthermore, they reveal that the differential effect of a *pasTI*/*ratAB* knockout in the two *E. coli* strains is not due to differences between PasT and its ortholog RatA. This finding is not unexpected given the near identity of PasT and RatA protein sequences with two amino acid differences only (S90 and D111 in PasT of *E. coli* CFT073, and N90 and E111 in *E. coli* K-12 MG1655). To clarify whether *E. coli* CFT073 or K-12 is representative of enterobacteria in general, we tested the ciprofloxacin tolerance phenotype of *pasTI* mutants constructed in two additional pathogenic *E. coli* strains and the more distantly related *Salmonella* Typhimurium (Figure A3, Appendix 2). Clearly, *pasTI* knockouts of *E. coli* O157:H7 strain EDL933 and *S. enterica* Typhimurium SR-11 showed decreased levels of ciprofloxacin-tolerant persisters that could be complemented by expression of *E. coli* CFT073 *pasT*. The other tested pathogenic *E. coli* strain 55989 also showed lower ciprofloxacin tolerance after *pasTI* was knocked out, but we cannot exclude that this phenotype might be partially caused by decreased intrinsic ciprofloxacin resistance of the *pasTI* mutant in this strain (Figure A3, Appendix 2). Taken together, these results suggest that the phenotypes of *E. coli* CFT073 Δ*pasTI* and not of *E. coli* K-12 Δ*ratAB* are more broadly representative.

3.3 | *E. coli* PasT/RatA is the homolog of mitochondrial Coq10

The *pasT*/*ratA* gene is well conserved among Proteobacteria and not always associated with *pasI*/*ratB* orthologs (Figure 3), suggesting that PasT/RatA might have a conserved housekeeping function that can be exerted independently of its previously proposed antitoxin partner.

Interestingly, PasT shares a protein domain (Pfam: Polyketide_cyc2, PF10604; InterPro: StART domain, IPR005031) and modest sequence similarity to the mitochondrial protein Coq10 (Figure A4a/b, Appendix 2; Shen et al., 2005; Tsui et al., 2019). Coq10 has been studied as an accessory factor of the mitochondrial electron transport chain (ETC), a series of protein complexes that create an electrochemical gradient across a membrane (the "proton-motive force") which fuels cellular ATP synthesis (Figure 4a; Anraku, 1988). In *E. coli*, electron transport along the ETC involves the electron shuttle ubiquinone under aerobic conditions (Sharma, Teixeira de Mattos, Hellingwerf, & Bekker, 2012) while two related but distinct molecules, menaquinone and demethylmenaquinone, predominate under anaerobic conditions (Nitzschke & Bettenbrock, 2018 and literature cited therein). Studies on yeast Coq10 indicated that this protein might serve as a "lipid chaperone" carrying newly synthesized ubiquinone to the respiratory complexes and/or localizing it properly within the ETC using a steroidogenic acute regulatory protein-related lipid transfer (StART) domain (Figure 4a; Awad et al., 2018; Tran & Clarke, 2007). Based on the similarity of the two proteins, we hypothesized that PasT/RatA might be the bacterial homolog of mitochondrial Coq10 and have a related or even equivalent role in cellular respiration.

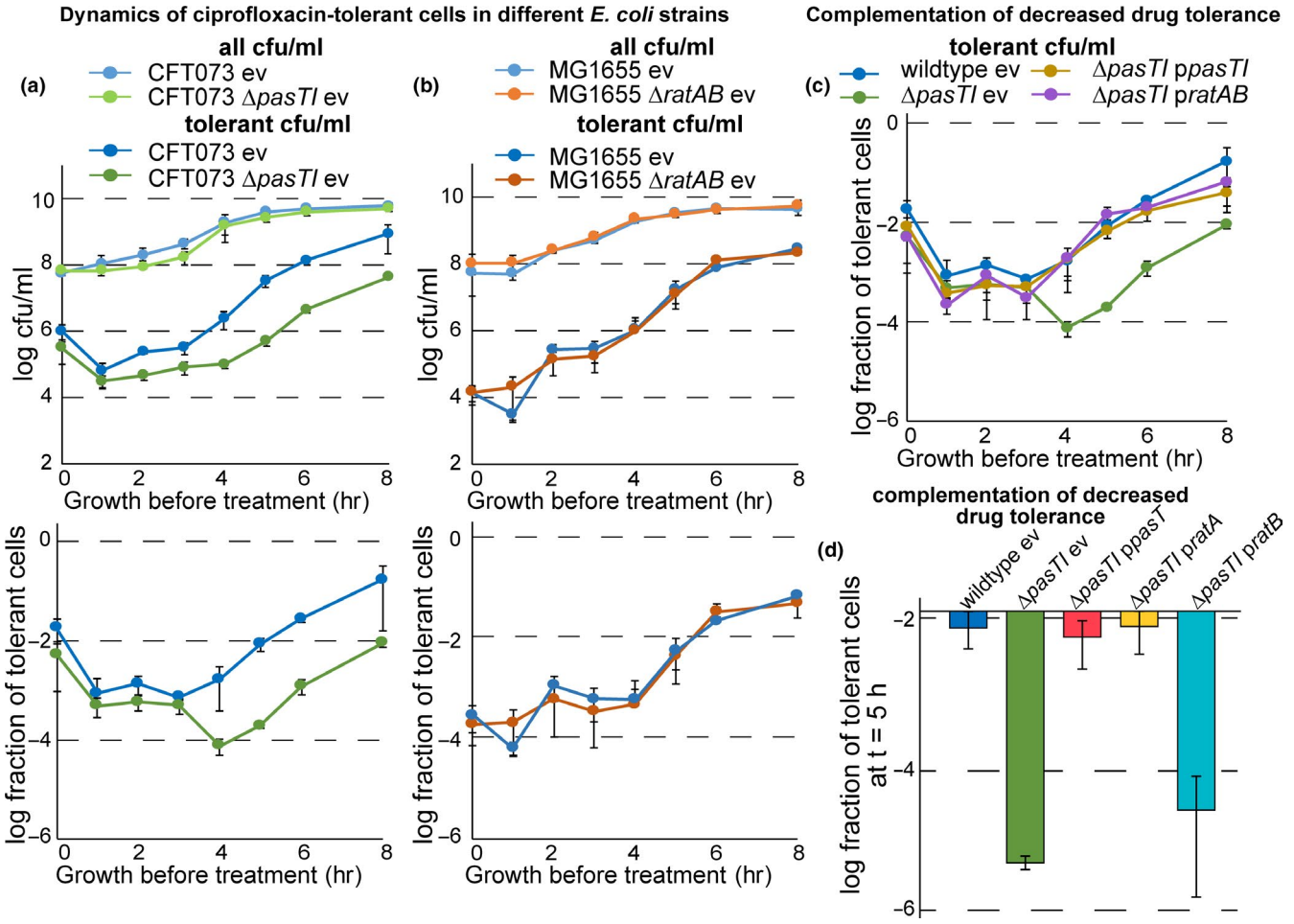

FIGURE 2 PasT is important for the formation or survival of ciprofloxacin-tolerant persisters. (a) Bacterial growth (colony-forming units (cfu)/ml; top graph) and dynamics of ciprofloxacin-tolerant cells (tolerant cfu/ml; top graph), as well as the fraction of tolerant cells at each data point (bottom graph), were determined for cultures of *E. coli* CFT073 and CFT073 Δ*pasTI* over time from inoculation over exponential growth into stationary phase. In short, bacteria were cultured for 1 hr, 2 hr, 3 hr, etc., and at each time point, we determined (1) total bacterial cfu/ml by direct plating and (2) drug-tolerant cfu/ml by plating after 5 hr of treatment with 10 μg/ml ciprofloxacin (see Materials and Methods for details). (b) The same experiment as described in (a) was performed for cultures of *E. coli* K-12 MG1655 and its Δ*ratAB* derivative. A similar drop of tolerance in *E. coli* CFT073 Δ*pasTI* (and the lack thereof in *E. coli* K-12 MG1655 Δ*ratAB*) was also observed for treatment with the membrane-targeting antibiotic colistin but not with the β-lactam ampicillin (Figure A2b/c in Appendix 2). Similar results as obtained with *E. coli* CFT073 and its Δ*pasTI* mutant in (a) were also obtained with different pathogenic *E. coli* strains and *Salmonella* Typhimurium (Figure A3a in Appendix 2). (c) Fractions of tolerant cells for cultures of *E. coli* CFT073 Δ*pasTI* harboring complementation plasmids encoding *pasTI* or *ratAB* as well as wild-type and Δ*pasTI* carrying the empty vector (ev) were determined as shown in (a). (d) The fraction of tolerant cells at 5 hr after inoculation was determined for cultures of *E. coli* CFT073 Δ*pasTI* harboring complementation plasmids encoding *pasT*, *ratA*, or *ratB*. Time–kill curves of all strains included in (a-d) sampled at this time point showed biphasic killing, demonstrating that the differences in surviving cfu/ml reflect different levels of persister cells (Figure A2a in Appendix 2). All data points in (a-d) represent the mean of results from at least three independent experiments, and error bars indicate standard deviations

3.4 | *E. coli ΔpasTI/ΔratAB* mutants display defective respiration and modest phenotypes in ubiquinone biosynthesis

Yeast mutants lacking *coq10* are known to display defective electron transport (Allan et al., 2013; Cui & Kawamukai, 2009), and we therefore studied whether ETC functionality is also compromised in *E. coli* mutants lacking PasT/RatA. The efficiency of bacterial electron transport was assessed using fluorescent indicator dye $DiOC_2(3)$ to probe the cellular membrane potential. Compared to the parental wild-type strains, both *pasTI* and *ratAB* mutants revealed a modest shift of signal toward the depolarized controls that could be complemented by providing *pasT* or *ratA in trans* (Figure 4b). As an independent approach to study the same phenomenon, we compared the minimum inhibitory concentrations (MICs) of gentamicin and zeocin for growth of the *E. coli pasTI* and *ratAB* mutants and their parental wild-type strains (Figure 4c,d; see also Figure A5a-c in Appendix 2). The uptake of gentamicin and zeocin, antibiotics of the aminoglycoside and the bleomycin families, is directly dependent on and proportional to the proton-motive force, so that impaired functionality

of the ETC results in an increased MIC of these antibiotics (Krause, Serio, Kane, & Connolly, 2016; Miller, Edberg, Mandel, Behar, & Steigbigel, 1980; Søballe & Poole, 2000). We indeed observed elevated MICs of both drugs for the *pasTI* and *ratAB* mutants that could be complemented with *pasT* or *ratA* but not *ratB* (Figure 4c,d; see also Figure A5a-c in Appendix 2). Taken together, these results suggest a clear but modest decrease in membrane polarization as a consequence of defective electron transport for both *E. coli* CFT073 Δ*pasTI* and *E. coli* K-12 MG1655 Δ*ratAB* mutants. Similar results were obtained with wild-type and Δ*pasTI* variants of different pathogenic *E. coli*/*S. enterica* strains (Figure A5d/e in Appendix 2).

To study the role of ubiquinone in these phenotypes, we quantified the total levels of ubiquinone and biosynthetic intermediates as well as the de novo biosynthesis of ubiquinone in *E. coli* Δ*pasTI*/Δ*ratAB* mutants (Figure 5a-d). Previous work found that yeast *coq10* mutants show decreased efficiency of ubiquinone biosynthesis specifically in exponential growth but have largely normal overall levels of ubiquinone in their mitochondria (Allan et al., 2013; Barros et al., 2005). Similarly, we saw no differences in total ubiquinone content when comparing *E. coli* Δ*pasTI*/Δ*ratAB* mutants to their parental wild-type strains (Figure 5b). However, we indeed found a decrease in ubiquinone precursor levels for both Δ*pasTI* and Δ*ratAB* mutants during the exponential growth phase and a mild defect in the de novo biosynthesis of ubiquinone specifically for CFT073 Δ*pasTI* in early log phase that could be complemented by *pasT*/*ratA* (Figure 5c/d).

3.5 | *E. coli ΔpasTI/ΔratAB* mutants display increased susceptibility to oxidative stress

Beyond defects in electron transport and log-phase ubiquinone biosynthesis, yeast mutants lacking Coq10 are known to be hypersensitive to oxidative stress (Allan et al., 2013; Cui & Kawamukai, 2009). This phenomenon is consistent with our observation that *E. coli* and *Salmonella pasTI* and *ratAB* mutants grow like their parental wild-types in the absence of oxygen but show a small-colony phenotype under aerobic conditions (Figure 6a; see also Figure A6a-b in Appendix 2). Similar phenotypes are typical for bacterial mutants with defects in respiration and/or ubiquinone biosynthesis and have also been described for the *pasT* knockout of *E. coli* CFT073 in previous work (Aussel et al., 2014; Day, 2013; Koskiniemi, Pranting, Gullberg, Näsvall, & Andersson, 2011; Norton & Mulvey, 2012; Poon et al., 2000; Proctor et al., 2014; Xia et al., 2017). Complementation with *pasT* or *ratA*, but not *ratB*, provided on a low-copy plasmid enabled the growth of *E. coli pasTI* and *ratAB* mutants to normal colony size under aerobic conditions (Figure 6b,c; see Figure A6a in Appendix 2).

We further compared the sensitivity of *E. coli* CFT073 Δ*pasTI* and its parental wild-type to hydrogen peroxide (H_2O_2) as an exogenous source of oxidative damage (Figure 7a). Similar to previous observations with yeast *coq10* mutants (Cui & Kawamukai, 2009), the *pasT* knockout was hypersensitive to oxidative damage which could be abolished by pretreating the cultures with the potent antioxidant ascorbic acid (vitamin C; Figure 7b and Figure A6c-e in Appendix 2). The H_2O_2 sensitivity of *E. coli* CFT073 Δ*pasTI* could also be complemented *in trans* by *pasT*/*ratA*, but not *ratB*, expressed from their promoter (Figure 7c). Taken together, these results presented in Figures 4-7 establish that the lack of PasT or RatA in *E. coli* causes similar phenotypes as known for yeast *coq10* mutants.

3.6 | PasT deficiency in *E. coli* can be functionally complemented with human mitochondrial Coq10

Given the high conservation of respiratory electron transport including the electron shuttle ubiquinone, we wondered whether PasT/RatA knockout phenotypes could be heterologously complemented by other bacterial or even mitochondrial homologs. Previous work had already shown that the alphaproteobacterial PasT homolog CC1376 of *C. crescentus* and human Coq10 can complement the *S. cerevisiae* Δ*coq10* phenotypes (Allan et al., 2013; Barros

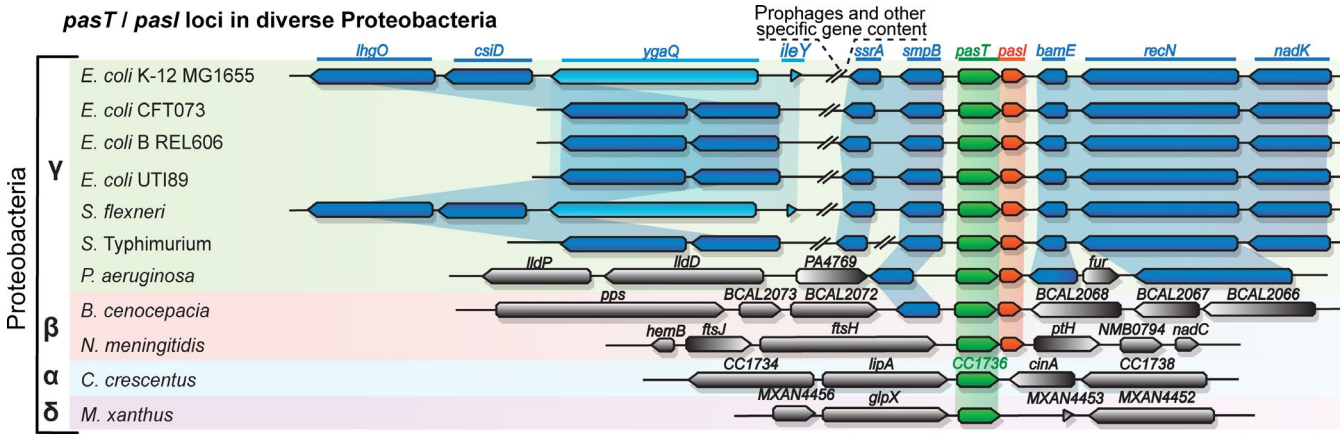

FIGURE 3 *pasT* and, to a lesser extent, *pasI* are widely conserved among Proteobacteria. The genomic organization of *pasT* (green)/*pasI* (orange) loci is shown for representative Proteobacteria. Genes conserved in two or more organisms are shown in blue. A list of full strain names and genome accessions used for this synteny analysis is found in Table A4 (Appendix 1).

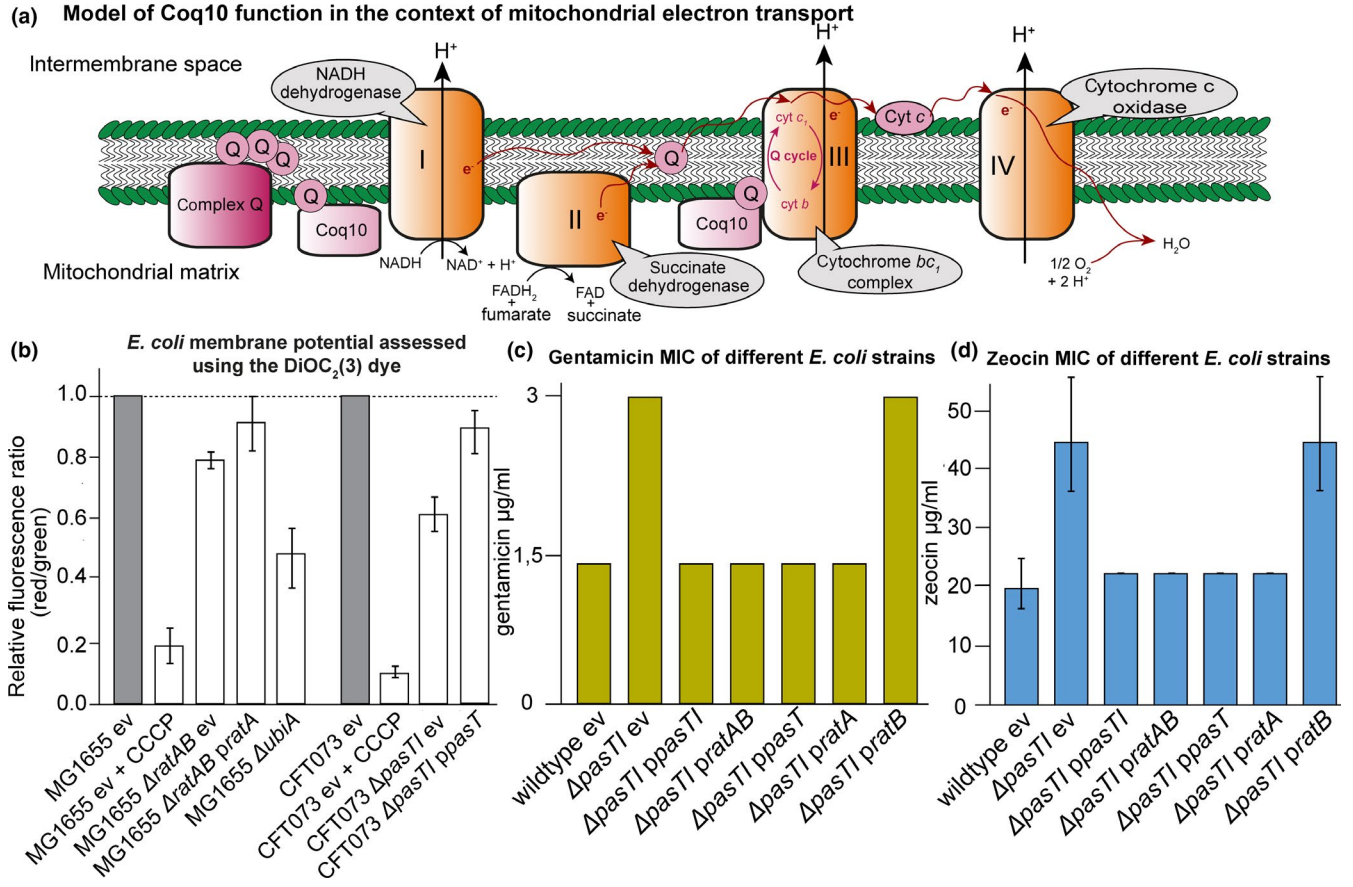

FIGURE 4 *E. coli* CFT073 Δ*pasTI* and *E. coli* MG1655 Δ*ratAB* mutants have a defective electron transport chain (ETC). (a) The figure illustrates how electrons (e^-) flow in the mitochondrial electron transport chain (ETC) from complex I (NADH dehydrogenase) or complex II (succinate dehydrogenase) to complex III (cytochrome bc_1 complex) via membrane-bound ubiquinone (commonly abbreviated as Q). Then, electrons transit via cytochrome C molecules and reach complex IV (cytochrome c oxidase) where they reduce dioxygen into water. Electron transfer is coupled to the active export of protons through the ETC complexes. The overall setup of this ETC is related in mitochondria and *E. coli*, but *E. coli* can also respire anaerobically by using alternative terminal electron acceptors and the dedicated anaerobic electron carriers menaquinone and demethylmenaquinone instead of ubiquinone. Studies on the mitochondrial ETC in yeast suggested that Coq10 is a "lipid chaperone" involved in the delivery of ubiquinone (synthesized by the multi-subunit protein complex Q) to its sites of function and/or proper localization at the sites of function (recently reviewed by Awad et al., 2018; Stefely & Pagliarini, 2017; Tran & Clarke, 2007). (b) The membrane potential of different *E. coli* samples was assessed using the $DiOC_2(3)$ dye in a way that a decrease in red/green ratio is indicative of depolarization (see Materials and Methods). Results were compared to values obtained with the uncoupler CCCP (complete depolarization) and the *E. coli* K-12 *ubiA* mutant (unable to synthesize ubiquinone; Pelosi et al., 2019). Both *ratAB* and—more pronounced—*pasTI* knockouts showed a decrease in the signal that was less strong than the effect of a *ubiA* knockout and could be complemented by *ratA*/*pasT*. (c, d) Minimum inhibitory concentrations (MIC) of *E. coli* CFT073 Δ*pasTI* for gentamicin (c) and zeocin (d) were determined by broth dilution assays. The bacteria carried either an empty vector (ev) or complementation plasmids encoding *pasTI*, *ratAB*, *pasT*, *ratA*, or *ratB*. For gentamicin, the result of one representative experiment is shown (additional independent replicates in Figure A5a in Appendix 2). Similar results were obtained for *E. coli* K-12 MG1655 Δ*ratAB*. (Figure A5b/c in Appendix 2). Unless specified otherwise, data points represent the mean of results from three independent experiments, and error bars indicate standard deviations.

et al., 2005; Cui & Kawamukai, 2009). Remarkably, both CC1376 and human mitochondrial Coq10 could also complement all phenotypes of RatA/PasT knockout mutants in *E. coli*: small colony size under aerobic condition, increased MIC of gentamicin/zeocin, defect of *E. coli* CFT073 in antibiotic tolerance, and, at least to some extent, H_2O_2 sensitivity (Figure 8a-d and Figure A6f in Appendix 2). These results show that RatA/PasT and CC1376 or Coq10 are not merely homologs (Figure A4a/b in Appendix 2) but seem to also share a function linked to respiratory electron transport that is conserved from bacteria to humans.

4 | DISCUSSION

4.1 | No evidence for links between PasT and PasI or a common function as a TA system

Our study had initially been inspired by previous work proposing that PasT is a TA-encoded toxin that inhibits ribosome assembly and somehow contributes to persister cell formation of uropathogenic *E. coli* (Norton & Mulvey, 2012; Zhang & Inouye, 2011). Given recent debates about the role of TA systems in antibiotic tolerance of *E. coli*,

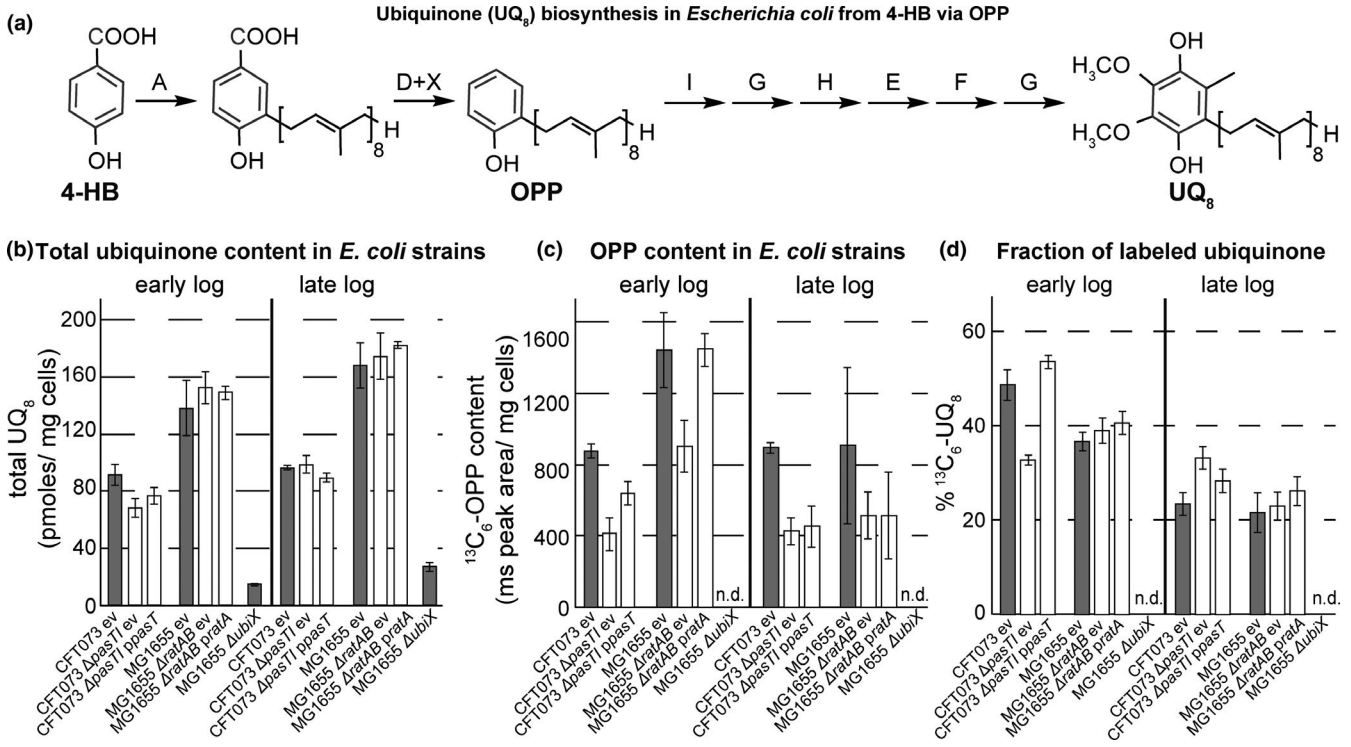

FIGURE 5 Direct measurements of ubiquinone levels and biosynthesis. (a) Schematic summary of the ubiquinone (UQ_8) biosynthetic pathway in *E. coli*. The precursor of 4-hydroxybenzoic acid (4-HB) is prenylated by UbiA and decarboxylated by UbiD to form the early intermediate octaprenyl-phenol (OPP). Subsequent modifications of the aromatic ring by Ubi enzymes (UbiI, UbiG, UbiH, UbiE, and UbiF) yield ubiquinone 8 (UQ_8). When $^{13}C_7$-4-HB is added to cultures to evaluate de novo synthesis of UQ, $^{13}C_6$-OPP and $^{13}C_6$-UQ_8 are formed (^{13}C carbon atoms represented in green). (b) Total ubiquinone (UQ_8) content (sum of $^{13}C_6$-UQ_8 and unlabeled ubiquinone UQ_8) was assessed after HPLC-ECD-MS analysis (see Materials and Methods) for early and late log-phase cultures of *E. coli* CFT073, K-12 MG1655, their Δ*pasTI*/Δ*ratAB* mutant derivatives, and the complemented strains. (c) The content of $^{13}C_6$-OPP (octaprenyl-phenol, an early intermediate of the UQ_8 pathway, see (a)) is reported for the same strains. (d) The plot shows the fraction of $^{13}C_6$-UQ_8 over total UQ_8 and is thus informative about the de novo biosynthesis of UQ_8 for the same strains as in (b) and (c). All data points represent the mean of results from four independent experiments, and error bars indicate standard deviations. An *E. coli* K-12 MG1655 *ubiX* mutant was used as a negative control in these experiments since UbiX is required for ubiquinone biosynthesis by producing a crucial cofactor for UbiD (Aussel et al., 2014; White et al., 2015; see also in (a)). ev = empty vector pNDM220, n.d. = not detected

this was a very interesting result (Goormaghtigh et al., 2018; Harms et al., 2017; Shan et al., 2017). However, we found no evidence for a link of PasT to either TA systems or ribosomes. Consistently, the data of a previous study also showed that expression of the PasT/RatA ortholog of *Salmonella* Typhimurium did not affect bacterial growth (Lobato-Marquez, Moreno-Cordoba, Figueroa, Diaz-Orejas, & Garcia-del Portillo, 2015). The discrepancy between our results and earlier work reporting growth inhibition upon PasT expression may be explained by the very high overexpression of protein constructs in previous studies that is prone to interfere with cellular physiology. Consistently, severe overexpression of *coq10* in yeast inhibited cellular growth by interfering with mitochondrial respiration (Zampol et al., 2010).

Our study also did not find evidence for a functional link between PasT and PasI, because phenotypes observed with Δ*pasTI* mutants could always be complemented by *pasT* and its homologs alone but never by its proposed antitoxin partner. Consistently, only *pasT* genes of beta- and gammaproteobacteria are accompanied by a *pasI* gene while solitary *pasT* (including mitochondrial *coq10*) is much more abundant (Figure 3; Shen et al., 2005; Tsui et al., 2019). Future studies could therefore explore whether PasI might be an accessory factor to PasT that constitutes an evolutionary innovation in beta- and gammaproteobacteria or whether *pasI* is just a functionally unrelated protein that these lineages acquired and encoded next to *pasT* merely by chance.

4.2 | Unification of the PasT/Coq10 family of StART domain proteins

Though we cannot exclude that PasT has a moonlighting function linked to ribosome assembly, multiple observations suggest that PasT is the bacterial equivalent of its mitochondrial homolog Coq10 that acts as an accessory factor in the ubiquinone-dependent ETC: *E. coli* mutants lacking PasT/RatA display phenotypes linked to defective ubiquinone-dependent electron transport that are similar to

phenotypes observed for *coq10* mutants (Figures 4-7), and these phenotypes can be largely complemented by human Coq10 (Figure 8). Consistently, a prediction of potential functional partners for PasT/RatA using STRING (https://string-db.org/; Szklarczyk et al., 2018) retrieved many proteins involved in ubiquinone biosynthesis and the ETC but no ribosomal proteins (Figure A4c in Appendix 2). From these results, we therefore conclude that PasT/RatA are not only homologous to Coq10 but at least to large extent functionally equivalent as "lipid chaperones" that arrange the utilization of ubiquinone in the ETC (recently reviewed by Awad et al., 2018; Stefely & Pagliarini, 2017).

These findings close one of the multiple gaps in our understanding of the electron transport chain and the functionality of ubiquinone that are widely conserved and thus relevant both for human diseases and—given the broad conservation of *pasT* among pathogenic Proteobacteria (Figure 3)—for antibiotic treatment (Aussel et al., 2014; Hirose et al., 2019; Stefely & Pagliarini, 2017). Notably, eukaryotic ubiquinone biosynthesis and respiratory electron transport chain are mitochondrial pathways that have been acquired by the eukaryotic lineage from the primordial bacterial endosymbiont during its evolution from a proteobacterium into extant mitochondria (Andersson et al., 1998; Stefely & Pagliarini, 2017). We therefore anticipate that future studies on the PasT/Coq10 family might use the technically highly accessible *E. coli* system to unravel the molecular function of these proteins in ubiquinone-dependent respiration that seems to be conserved from bacteria to humans.

4.3 | Links between PasT, electron transport, and oxidative stress

E. coli Δ*ratAB*/Δ*pasTI* mutants display several phenotypes linked to oxidative stress sensitivity or redox balance (Figure 4 and Figure 6/Figure 7) that correlates with modest defects in exponential-phase ubiquinone biosynthesis as also previously observed for yeast *coq10* mutants (see above). However, it is not clear how defective respiration causes these phenotypes or what is the molecular function of Coq10 (Allan et al., 2013; Awad et al., 2018; Barros et al., 2005; Cui & Kawamukai, 2009; Stefely & Pagliarini, 2017; Tsui et al., 2019). In this regard, our study moves the understanding of PasT/RatA roughly to the point of how far the field understands Coq10.

Notably, the mild defect of *E. coli* CFT073 Δ*pasTI* in ubiquinone biosynthesis (Figure 5c/d) was too weak to affect steady-state ubiquinone levels (Figure 5a). It therefore cannot explain the multiple phenotypes of *E. coli* Δ*pasTI*/Δ*ratAB* mutants that are linked to defective aerobic respiration given that, for example, the considerable reduction of ubiquinone levels in an *E. coli ubiI* mutant (ca. 15% of wild-type) still enables normal respiration (Pelosi et al., 2016). These strong pleiotropic phenotypes of PasT/RatA deficiency (and the lack of Coq10) are therefore likely caused by problems linked to the proposed role of these proteins as "lipid chaperones" that facilitate the implementation of ubiquinone at the electron transport chain (recently reviewed by Awad et al., 2018; Stefely & Pagliarini, 2017). Consequently, the observed phenotypes in ubiquinone biosynthesis

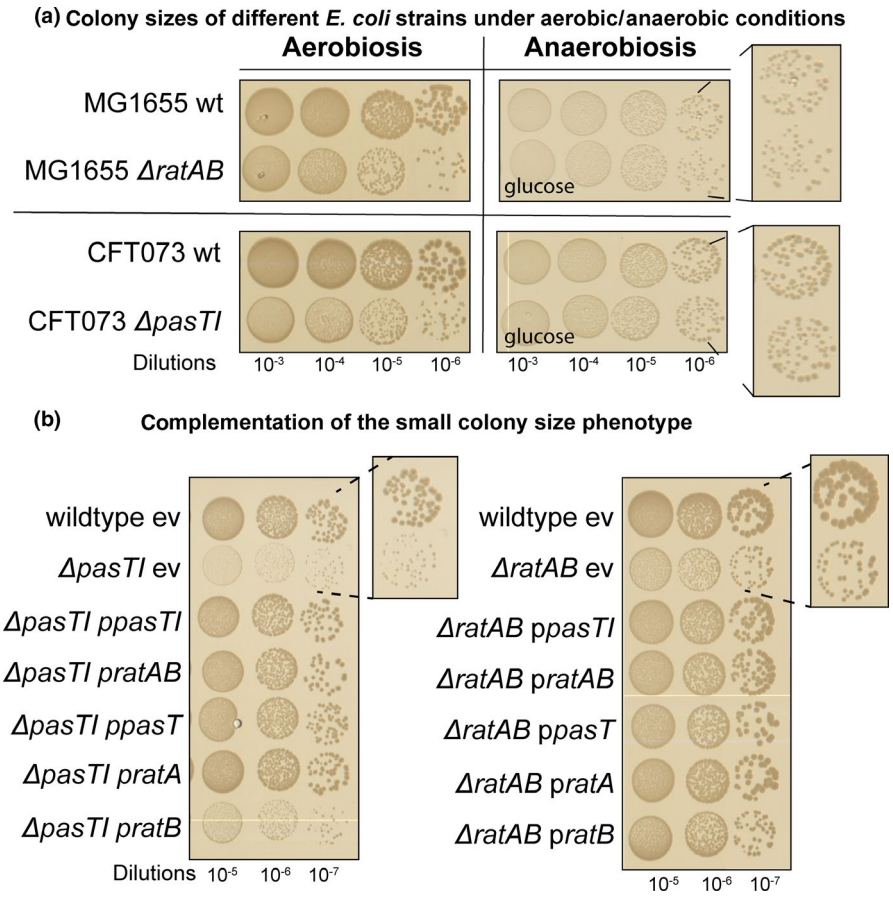

FIGURE 6 Lack of *pasT*/*ratA* causes a small-colony phenotype under aerobic conditions. (a) Cultures of *E. coli* CFT073 wild-type, *E. coli* K-12 MG1655 wild-type, and their Δ*pasTI*/Δ*ratAB* derivatives were diluted and spotted on LB agar plates incubated either in the presence (left) or absence (right) of oxygen. D-glucose (1% w/v) was added as a fermentable carbon source to LB agar plates incubated anaerobically (see Materials and Methods). (b, c) Spot assay of *E. coli* CFT073 Δ*pasTI* (b) or *E. coli* K-12 MG1655 Δ*ratAB* (c) carrying the empty vector (ev) or different complementation plasmids was spotted on LB agar plates to visualize differences in colony size. Similar results as shown in (a-c) were also obtained with different pathogenic *E. coli* strains and *Salmonella* Typhimurium (Figure A6a/b in Appendix 2)

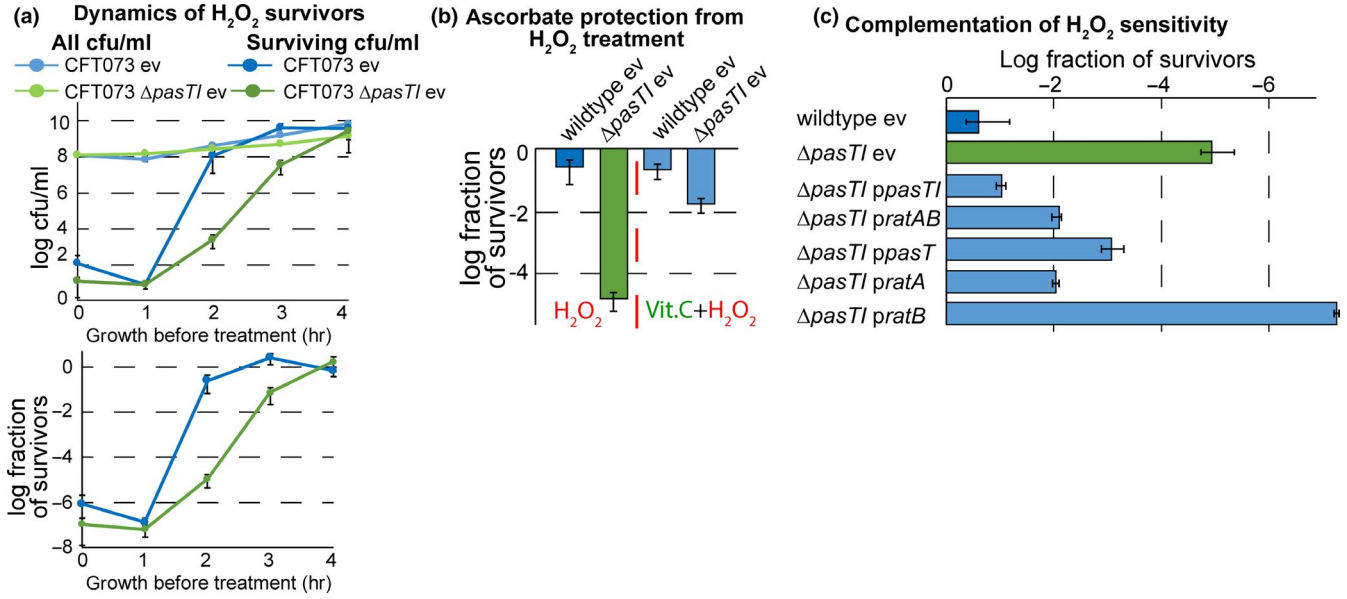

FIGURE 7 *pasT*/*ratA* deficiency causes hypersensitivity to redox stress and oxidative damage in *E. coli*. (a) Dynamics of colony-forming units (cfu/ml: top graph; a fraction of survivors: bottom graph) before and after treatment with hydrogen peroxide (H_2O_2) for *E. coli* CFT073 wild-type/Δ*pasTI* over time after inoculation from stationary phase into fresh medium (see Materials and Methods). (b) The fraction of cells surviving H_2O_2 treatment 2 hr after inoculation from the stationary phase was determined for cultures of *E. coli* CFT073 wild-type/Δ*pasTI* with or without pretreatment with the antioxidant vitamin C (ascorbate). Similar results as shown in (a) and (b) for *E. coli* CFT073 wild-type/Δ*pasTI* were also obtained for *E. coli* K-12 MG1655 wild-type/Δ*ratAB* (Figure A6d/e in Appendix 2). (c) The fraction of cells surviving H_2O_2 treatment 2 hr after inoculation from stationary phase was determined for cultures of *E. coli* CFT073 wild-type/Δ*pasTI* carrying either the empty vector (ev) or different complementation plasmids. We could not assay the complementation of H_2O_2 sensitivity for *E. coli* K-12 MG1655 Δ*ratAB* because, curiously, already the empty vector caused a strong decrease in H_2O_2 sensitivity of this strain (Figure A6d in Appendix 2). All data points in (a-c) represent the mean of results from at least three independent experiments, and error bars indicate standard deviations

might rather be downstream consequences—maybe via a feedback mechanism—of improperly utilized ubiquinone.

In general, impaired aerobic respiration often causes growth defects and a small-colony phenotype specifically under aerobic conditions (Aussel et al., 2014; Day, 2013; Koskiniemi et al., 2011; Poon et al., 2000; Proctor et al., 2014; Xia et al., 2017). On the one hand, this observation could be explained by the poor energy metabolism of these mutants due to their limited ability to use oxygen as a terminal electron acceptor, while under anaerobic conditions other quinone electron shuttles serve other terminal acceptors or merely fermentation takes place instead. On the other hand, these observations could be explained as a consequence of reactive oxygen species (ROS) sensitivity and/or production. Consistently, *E. coli* K-12 defective for ubiquinone production grows poorly under aerobic conditions where it shows signs of oxidative stress (Nitzschke & Bettenbrock, 2018), and similar observations have been made for a yeast *coq10* mutant (Cui & Kawamukai, 2009). These results could be explained by the pro- and antioxidant activities of different forms of ubiquinone, but the details of this relationship have not been resolved (Wang & Hekimi, 2016). Also, defects in the electron transport chain cause leakage of electrons and uncontrolled formation of ROS that damages cellular macromolecules, a problem inherent to respiration, and linked to many human diseases (Jastroch, Divakaruni, Mookerjee, Treberg, & Brand, 2010). We anticipate that future studies unraveling the precise biological function of PasT/Coq10 in the context of ubiquinone-dependent respiration will also reveal how the lack of its activity is linked to oxidative stress and cellular redox balance in bacteria and humans.

4.4 | PasT highlights the importance of electron transport for bacterial persister cells

The initial focus of our study was to understand the specific defect of uropathogenic *E. coli* CFT073 lacking *pasTI* in the formation or survival of persister cells (Norton & Mulvey, 2012). We readily reproduced this phenotype in *E. coli* CFT073 itself and different pathogenic *E. coli* strains as well as *Salmonella* Typhimurium (Figure 2 as well as Figures A2 and A3 in Appendix 2). However, our results also showed that PasTI is not just a genetic switch controlling transition into dormancy as a TA module would supposedly be. Instead, PasT seems to be deeply wired into bacterial redox balance and energy metabolism through its role as a facilitator of ubiquinone-dependent respiration (Figure 9). The link of PasT to antibiotic tolerance is therefore likely indirect and mediated through broad distortions of bacterial physiology caused by defective aerobic respiration.

A general link between persister formation and ETC functionality is well established; various mutations in ETC components can show both increased and decreased levels of persisters (Harms et al., 2016; Shan, Lazinski, Rowe, Camilli, & Lewis, 2015; Van den

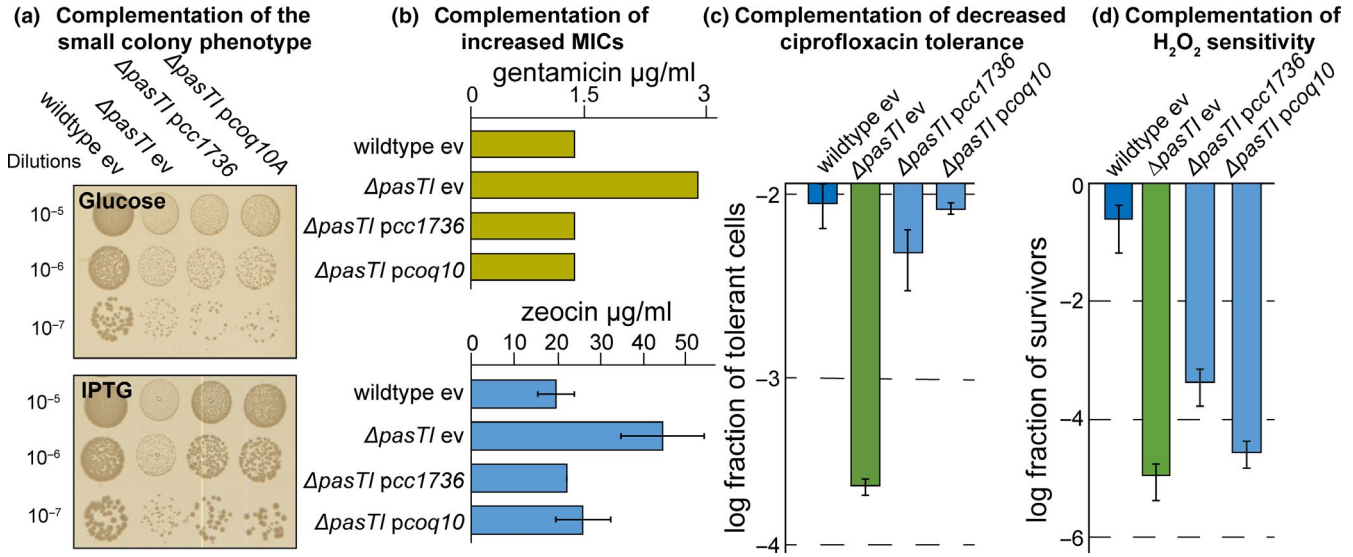

FIGURE 8 CC1736 of *Caulobacter crescentus* and human mitochondrial Coq10 can functionally complement the *E. coli* CFT073 Δ*pasTI* mutant. (a) The colony sizes of *E. coli* CFT073 strain harboring the empty vector (ev) or complementation plasmids encoding *pasT* homolog *cc1736* from *C. crescentus* or human *coq10* under P*lac* control were analyzed on LB agar plates supplemented with 1% D-glucose (repressing expression of complementation constructs) or 1 mM IPTG (inducing expression of complementation plasmids). Similar results were obtained with *E. coli* K-12 MG1655 Δ*ratAB* (Figure A6f in Appendix 2). (b) Minimum inhibitory concentration (MIC) of these strains for gentamicin (top) and zeocin (bottom) was determined via broth dilution assays. For gentamicin, results of one representative experiment are presented; additional independent replicates and similar data obtained with *E. coli* K-12 MG1655 Δ*ratAB* are shown in Appendix 2 (Figure A5a-c). (c) Antibiotic tolerance assays were performed like those shown in Figure 2, and the fraction of ciprofloxacin-tolerant cells 5 hr after inoculation was determined for cultures of *E. coli* CFT073 Δ*pasTI* harboring complementation plasmids encoding *cc1736* or *coq10* or the empty vector (ev). Time–kill curves at this time point showed biphasic killing, revealing that the differences in antibiotic tolerance reflect different levels of persister cells (Figure A2a in Appendix 2). (d) The sensitivity of *E. coli* CFT073 Δ*pasTI* to treatment with hydrogen peroxide (H_2O_2) 2 hr after inoculation was determined for strains carrying *cc1736* or *coq10* complementation plasmids or the empty vector (ev) as shown in Figure 7c. Unless indicated otherwise, all data points in (a-d) represent the mean of results from at least three independent experiments and error bars indicate standard deviations. In all experiments, the P*lac* promoter on all plasmids was induced during overnight cultures and throughout the experiment by supplementing culture media with 1 mM IPTG.

Bergh et al., 2016). However, the physiological basis of this link and the underlying molecular mechanisms are poorly understood. One possibility is that the ETC could modulate persister levels by affecting ATP production since persister formation can be associated with decreased ATP levels (Shan et al., 2017). However, impaired electron transport upon PasT deficiency should then rather cause increased persister formation by limiting cellular ATP production. Alternatively, it has been hypothesized repeatedly that bacterial killing by various antibiotics is causally linked to the generation of ROS by a hyperactivated ETC in response to metabolic perturbations (Kohanski, Dwyer, & Collins, 2010; Yang, Bening, & Collins, 2017), though these ideas have been disputed by others (Keren, Wu, Inocencio, Mulcahy, & Lewis, 2013; Liu & Imlay, 2013). This view would suggest that the decreased antibiotic tolerance upon *pasT* deficiency is linked to drug-induced ROS production and ultimately rooted in a general hypersensitivity to ROS. Consistently, mechanisms involved in reducing oxidative stress and increasing ROS detoxification have been linked previously to persister survival in *E. coli* CFT073 and other bacteria (Molina-Quiroz, Lazinski, Camilli, & Levy, 2016; Nguyen et al., 2011).

Critically, none of these hypotheses can explain why the four *E. coli* strains investigated in this work as well as *Salmonella* Typhimurium share most phenotypes linked to *pasT/ratA* deficiency except for the persister defect that is specifically absent in the *E. coli* K-12 MG1655 laboratory strain (Figure 2/Figure 4/Figure 6/Figure 7 and Figure A2/Figure A3/Figure A5/Figure A6 in Appendix 2). Also, the *E. coli* K-12 Δ*ratAB* mutant did not show the modest defect in exponential-phase ubiquinone biosynthesis that was readily apparent for *E. coli* CFT073 Δ*pasTI* (Figure 5d). Before testing the other strains beyond *E. coli* K-12 and CFT073, we initially suspected that the widespread use of strains carrying *rpoS* loss-of-function alleles ($rpoS_{am}$) as *E. coli* CFT073 "wild-type" might explain the increased sensitivity of this strain compared to K-12 MG1655 (Hryckowian, Baisa, Schwartz, & Welch, 2015; Hryckowian & Welch, 2013) since RpoS is a central player in *E. coli* stress responses (Battesti, Majdalani, & Gottesman, 2011). Targeted sequencing of *rpoS* indeed confirmed that our *E. coli* CFT073 strain carried the $rpoS_{am}$ allele. However, control experiments with a variant carrying intact *rpoS* found no differences in antibiotic tolerance and all other phenotypes to our original data beyond a change in the dynamics of H_2O_2 survival that in this strain look much more similar to *E. coli* K-12 MG1655 (Figure A7 in Appendix 2). These results suggest that RpoS-controlled stress responses can buffer against some of the distortions of bacterial physiology that are caused by a lack of PasT but do not explain

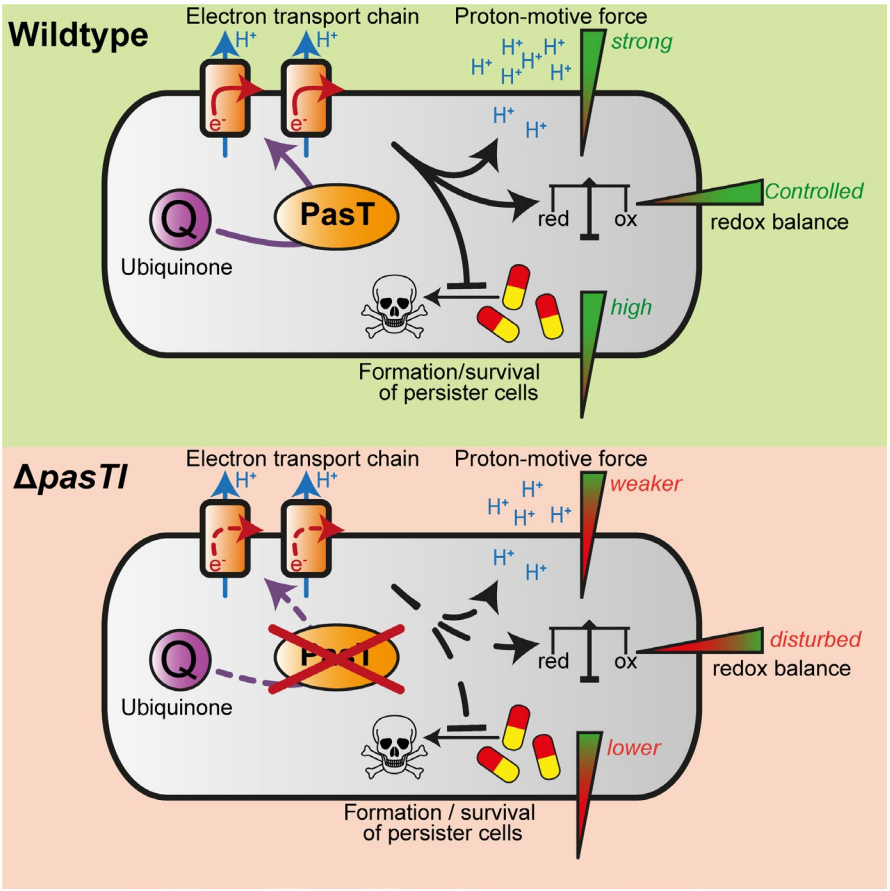

FIGURE 9 Working model: *pasT* deficiency causes pleiotropic phenotypes by interfering with ubiquinone-dependent respiration. The illustration summarizes and interprets the main results of our study. In the absence of PasT, membrane potential, resilience to oxidative stress, and (for pathogenic *E. coli* as well as *Salmonella* Typhimurium) levels of antibiotic-tolerant persisters are reduced (Figure 2/Figures 4-7 and Figure A2/Figure A3/Figure A5/Figure A6 in Appendix 2). These phenotypes are—similar to findings for yeast *coq10* mutants—likely caused by defective aerobic respiration due to impaired ubiquinone functionality at the electron transport chain (Figure 4/Figure 8)

the severe defect of *E. coli* CFT073 Δ*pasTI* in antibiotic tolerance. Given that this defect and all other phenotypes are also shared by different pathogenic *E. coli* as well as *Salmonella* Typhimurium (Figure A3/Figure A5/Figure A6 in Appendix 2), it is likely to be more representative of enterobacteria while the divergent behavior of *E. coli* K-12 MG1655 might be related to one or more features of the peculiar physiology of this laboratory-adapted strain (Hobman, Penn, & Pallen, 2007).

ACKNOWLEDGMENTS

The authors are grateful to Nick R. Thomson, Eva Heinz, Gal Horesh, and Anders Løbner-Olesen for valuable input and critical reading of the manuscript. *Escherichia coli* strain CFT073 with and without the inactive $rpoS_{am}$ allele was generously shared by Anders Løbner-Olesen and Daniel R. Brown, respectively. *Escherichia coli* strain 55989 and *Salmonella enterica* serovar *enterica* Typhimurium SR-11 were obtained from Karen A. Krogfelt, and an attenuated variant of *E. coli* O157:H7 strain EDL933 was obtained from Anders Løbner-Olesen. This work was supported by Danish National Research Foundation (DNRF) grant DNRF120 and a Novo Nordisk Foundation Laureate Research Grant (to K.G.). A.H. was supported by the European Molecular Biology Organization (EMBO) Long-Term Fellowship ALTF 564-2016 and Swiss National Science Foundation (SNSF) Ambizione Fellowship PZ00P3_180085.

CONFLICT OF INTEREST

None declared.

AUTHOR CONTRIBUTIONS

Cinzia Fino: Conceptualization (supporting); data curation (lead); formal analysis (lead); investigation (lead); validation (equal); visualization (equal); methodology (equal); resources (equal); writing—original draft preparation (equal); writing—review and editing (equal). **Martin Vestergaard:** Data curation (supporting); formal analysis (supporting); investigation (supporting); resources (supporting); methodology (supporting); writing—original draft preparation (supporting); writing—review and editing (supporting). **Hanne Ingmer:** Conceptualization (supporting); writing—review and editing (supporting); funding acquisition (supporting); supervision (supporting). **Fabien Pierrel:** Conceptualization (supporting); data curation (supporting); formal analysis (supporting); funding acquisition (supporting); investigation (supporting); methodology (supporting); resources (supporting); writing—original draft preparation (supporting); writing—review and editing (supporting). **Kenn Gerdes:** Conceptualization (equal); data curation (equal); funding acquisition (lead); project administration (lead); supervision (equal); writing—original draft (equal); writing—review and editing (equal). **Alexander Harms:** Conceptualization (equal); data curation (equal); formal analysis (equal); funding acquisition (equal); investigation (equal); methodology (equal); project administration

(equal); resources (equal); supervision (equal); validation (equal); visualization (equal); writing—original draft (equal); writing—review and editing (equal).

ETHICS STATEMENT

None required.

DATA AVAILABILITY STATEMENT

All data generated or analyzed during this study are included in this published article.

ORCID

Cinzia Fino https://orcid.org/0000-0002-6440-1976
Kenn Gerdes https://orcid.org/0000-0002-7462-4612
Alexander Harms https://orcid.org/0000-0003-2106-1286

REFERENCES

Allan, C. M., Hill, S., Morvaridi, S., Saiki, R., Johnson, J. S., Liau, W.-S., … Clarke, C. F. (2013). A conserved START domain coenzyme Q-binding polypeptide is required for efficient Q biosynthesis, respiratory electron transport, and antioxidant function in *Saccharomyces cerevisiae*. *Biochimica et Biophysica Acta*, *1831*(4), 776–791. https://doi.org/10.1016/j.bbalip.2012.12.007

Anderson, G. G., Palermo, J. J., Schilling, J. D., Roth, R., Heuser, J., & Hultgren, S. J. (2003). Intracellular bacterial biofilm-like pods in urinary tract infections. *Science*, *301*(5629), 105–107. https://doi.org/10.1126/science.1084550

Andersson, S. G. E., Zomorodipour, A., Andersson, J. O., Sicheritz-Pontén, T., Alsmark, U. C. M., Podowski, R. M., … Kurland, C. G. (1998). The genome sequence of *Rickettsia prowazekii* and the origin of mitochondria. *Nature*, *396*(6707), 133–140. https://doi.org/10.1038/24094

Anraku, Y. (1988). Bacterial electron transport chains. *Annual Review of Biochemistry*, *57*, 101–132. https://doi.org/10.1146/annurev.bi.57.070188.000533

Arndt, D., Grant, J. R., Marcu, A., Sajed, T., Pon, A., Liang, Y., & Wishart, D. S. (2016). PHASTER: A better, faster version of the PHAST phage search tool. *Nucleic Acids Research*, *44*(W1), W16–W21. https://doi.org/10.1093/nar/gkw387

Aussel, L., Loiseau, L., Hajj Chehade, M., Pocachard, B., Fontecave, M., Pierrel, F., & Barras, F. (2014). *ubiJ*, a new gene required for aerobic growth and proliferation in macrophage, is involved in coenzyme Q biosynthesis in *Escherichia coli* and *Salmonella enterica* serovar Typhimurium. *Journal of Bacteriology*, *196*(1), 70–79. https://doi.org/10.1128/JB.01065-13

Awad, A. M., Bradley, M. C., Fernandez-Del-Rio, L., Nag, A., Tsui, H. S., & Clarke, C. F. (2018). Coenzyme Q10 deficiencies: Pathways in yeast and humans. *Essays in Biochemistry*, *62*(3), 361–376. https://doi.org/10.1042/EBC20170106

Balaban, N. Q., Helaine, S., Lewis, K., Ackermann, M., Aldridge, B., Andersson, D. I., … Zinkernagel, A. (2019). Definitions and guidelines for research on antibiotic persistence. *Nature Reviews Microbiology*, *17*(7), 441–448. https://doi.org/10.1038/s41579-019-0196-3

Barros, M. H., Johnson, A., Gin, P., Marbois, B. N., Clarke, C. F., & Tzagoloff, A. (2005). The *Saccharomyces cerevisiae* COQ10 gene encodes a START domain protein required for function of coenzyme Q in respiration. *Journal of Biological Chemistry*, *280*(52), 42627–42635. https://doi.org/10.1074/jbc.M510768200

Battesti, A., Majdalani, N., & Gottesman, S. (2011). The RpoS-mediated general stress response in *Escherichia coli*. *Annual Review of Microbiology*, *65*, 189–213. https://doi.org/10.1146/annurev-micro-090110-102946

Blango, M. G., & Mulvey, M. A. (2010). Persistence of uropathogenic *Escherichia coli* in the face of multiple antibiotics. *Antimicrobial Agents and Chemotherapy*, *54*(5), 1855–1863. https://doi.org/10.1128/AAC.00014-10

Blank, K., Hensel, M., & Gerlach, R. G. (2011). Rapid and highly efficient method for scarless mutagenesis within the *Salmonella enterica* chromosome. *PLoS One*, *6*(1), e15763. https://doi.org/10.1371/journal.pone.0015763

Castro-Roa, D., Garcia-Pino, A., De Gieter, S., van Nuland, N. A. J., Loris, R., & Zenkin, N. (2013). The Fic protein Doc uses an inverted substrate to phosphorylate and inactivate EF-Tu. *Nature Chemical Biology*, *9*(12), 811–817. https://doi.org/10.1038/nchembio.1364

Chung, C. T., Niemela, S. L., & Miller, R. H. (1989). One-step preparation of competent *Escherichia coli*: Transformation and storage of bacterial cells in the same solution. *Proceedings of the National Academy of Sciences of the United States of America*, *86*(7), 2172–2175. https://doi.org/10.1073/pnas.86.7.2172

Cui, T. Z., & Kawamukai, M. (2009). Coq10, a mitochondrial coenzyme Q binding protein, is required for proper respiration in *Schizosaccharomyces pombe*. *FEBS Journal*, *276*(3), 748–759. https://doi.org/10.1111/j.1742-4658.2008.06821.x

Day, M. (2013). Yeast petites and small colony variants: For everything there is a season. *Advances in Applied Microbiology*, *85*, 1–41. https://doi.org/10.1016/B978-0-12-407672-3.00001-0

Dörr, T., Vulic, M., & Lewis, K. (2010). Ciprofloxacin causes persister formation by inducing the TisB toxin in *Escherichia coli*. *PLoS Biology*, *8*(2), e1000317. https://doi.org/10.1371/journal.pbio.1000317

Fauvart, M., De Groote, V. N., & Michiels, J. (2011). Role of persister cells in chronic infections: Clinical relevance and perspectives on anti-persister therapies. *Journal of Medical Microbiology*, *60*(Pt 6), 699–709. https://doi.org/10.1099/jmm.0.030932-0

Flores-Mireles, A. L., Walker, J. N., Caparon, M., & Hultgren, S. J. (2015). Urinary tract infections: Epidemiology, mechanisms of infection and treatment options. *Nature Reviews Microbiology*, *13*(5), 269–284. https://doi.org/10.1038/nrmicro3432

Germain, E., Castro-Roa, D., Zenkin, N., & Gerdes, K. (2013). Molecular mechanism of bacterial persistence by HipA. *Molecular Cell*, *52*(2), 248–254. https://doi.org/10.1016/j.molcel.2013.08.045

Glover, M., Moreira, C. G., Sperandio, V., & Zimmern, P. (2014). Recurrent urinary tract infections in healthy and nonpregnant women. *Urological Science*, *25*(1), 1–8. https://doi.org/10.1016/j.urols.2013.11.007

Goneau, L. W., Yeoh, N. S., MacDonald, K. W., Cadieux, P. A., Burton, J. P., Razvi, H., & Reid, G. (2014). Selective target inactivation rather than global metabolic dormancy causes antibiotic tolerance in uropathogens. *Antimicrobial Agents and Chemotherapy*, *58*(4), 2089–2097. https://doi.org/10.1128/AAC.02552-13

Goormaghtigh, F., Fraikin, N., Putrins, M., Hallaert, T., Hauryliuk, V., Garcia-Pino, A., … Van Melderen, L. (2018). Reassessing the role of type II toxin-antitoxin systems in formation of *Escherichia coli* type II persister cells. *Mbio*, *9*(3), e00640-18. https://doi.org/10.1128/mBio.00640-18

Gotfredsen, M., & Gerdes, K. (1998). The *Escherichia coli relBE* genes belong to a new toxin-antitoxin gene family. *Molecular Microbiology*, *29*(4), 1065–1076. https://doi.org/10.1046/j.1365-2958.1998.00993.x

Hajj Chehade, M., Pelosi, L., Fyfe, C. D., Loiseau, L., Rascalou, B., Brugière, S., … Pierrel, F. (2019). A soluble metabolon synthesizes the isoprenoid lipid ubiquinone. *Cell Chemistry & Biology*, *26*(4), 482–492.e7. https://doi.org/10.1016/j.chembiol.2018.12.001

Harms, A., Brodersen, D. E., Mitarai, N., & Gerdes, K. (2018). Toxins, targets, and triggers: An overview of toxin-antitoxin biology. *Molecular Cell*, *70*(5), 768–784. https://doi.org/10.1016/j.molcel.2018.01.003

Harms, A., Fino, C., Sørensen, M. A., Semsey, S., & Gerdes, K. (2017). Prophages and growth dynamics confound experimental results with antibiotic-tolerant persister cells. *Mbio*, *8*(6), e01964-17.https://doi.org/10.1128/mBio.01964-17

Harms, A., Maisonneuve, E., & Gerdes, K. (2016). Mechanisms of bacterial persistence during stress and antibiotic exposure. *Science*, *354*(6318), aaf4268. https://doi.org/10.1126/science.aaf4268

Helaine, S., Cheverton, A. M., Watson, K. G., Faure, L. M., Matthews, S. A., & Holden, D. W. (2014). Internalization of *Salmonella* by macrophages induces formation of nonreplicating persisters. *Science*, *343*(6167), 204–208. https://doi.org/10.1126/science.1244705

Hirose, K., Chang, S., Yu, H., Wang, J., Barca, E., Chen, X., Huang, G. N. (2019). Loss of a novel striated muscle-enriched mitochondrial protein Coq10a enhances postnatal cardiac hypertrophic growth. *bioRxiv*.

Hobman, J. L., Penn, C. W., & Pallen, M. J. (2007). Laboratory strains of *Escherichia coli*: Model citizens or deceitful delinquents growing old disgracefully? *Molecular Microbiology*, *64*(4), 881–885. https://doi.org/10.1111/j.1365-2958.2007.05710.x

Hryckowian, A. J., Baisa, G. A., Schwartz, K. J., & Welch, R. A. (2015). *dsdA* does not affect colonization of the murine urinary tract by *Escherichia coli* CFT073. *PLoS One*, *10*(9), e0138121. https://doi.org/10.1371/journal.pone.0138121

Hryckowian, A. J., & Welch, R. A. (2013). RpoS contributes to phagocyte oxidase-mediated stress resistance during urinary tract infection by *Escherichia coli* CFT073. *MBio*, *4*(1), e00023-00013. https://doi.org/10.1128/mBio.00023-13

Jahn, M., Vorpahl, C., Hubschmann, T., Harms, H., & Muller, S. (2016). Copy number variability of expression plasmids determined by cell sorting and Droplet Digital PCR. *Microbial Cell Factories*, *15*(1), 211. https://doi.org/10.1186/s12934-016-0610-8

Jastroch, M., Divakaruni, A. S., Mookerjee, S., Treberg, J. R., & Brand, M. D. (2010). Mitochondrial proton and electron leaks. *Essays in Biochemistry*, *47*, 53–67. https://doi.org/10.1042/bse0470053

Kelley, L. A., Mezulis, S., Yates, C. M., Wass, M. N., & Sternberg, M. J. (2015). The Phyre2 web portal for protein modeling, prediction and analysis. *Nature Protocols*, *10*(6), 845–858. https://doi.org/10.1038/nprot.2015.053

Keren, I., Wu, Y., Inocencio, J., Mulcahy, L. R., & Lewis, K. (2013). Killing by bactericidal antibiotics does not depend on reactive oxygen species. *Science*, *339*(6124), 1213–1216. https://doi.org/10.1126/science.1232688

Kohanski, M. A., Dwyer, D. J., & Collins, J. J. (2010). How antibiotics kill bacteria: From targets to networks. *Nature Reviews Microbiology*, *8*(6), 423–435. https://doi.org/10.1038/nrmicro2333

Koskiniemi, S., Pranting, M., Gullberg, E., Näsvall, J., & Andersson, D. I. (2011). Activation of cryptic aminoglycoside resistance in *Salmonella enterica*. *Molecular Microbiology*, *80*(6), 1464–1478. https://doi.org/10.1111/j.1365-2958.2011.07657.x

Krause, K. M., Serio, A. W., Kane, T. R., & Connolly, L. E. (2016). Aminoglycosides: An overview. *Cold Spring Harbor Perspectives in Medicine*, *6*(6), a027029. https://doi.org/10.1101/cshperspect.a027029

Lee, E.-C., Yu, D., Martinez de Velasco, J., Tessarollo, L., Swing, D. A., Court, D. L., … Copeland, N. G. (2001). A highly efficient *Escherichia coli*-based chromosome engineering system adapted for recombinogenic targeting and subcloning of BAC DNA. *Genomics*, *73*(1), 56–65. https://doi.org/10.1006/geno.2000.6451

Lewis, K. (2010). Persister cells. *Annual Review of Microbiology*, *64*, 357–372. https://doi.org/10.1146/annurev.micro.112408.134306

Liu, H., & Naismith, J. H. (2008). An efficient one-step site-directed deletion, insertion, single and multiple-site plasmid mutagenesis protocol. *BMC Biotechnology*, *8*, 91. https://doi.org/10.1186/1472-6750-8-91

Liu, Y., & Imlay, J. A. (2013). Cell death from antibiotics without the involvement of reactive oxygen species. *Science*, *339*(6124), 1210–1213. https://doi.org/10.1126/science.1232751

Lobato-Marquez, D., Moreno-Cordoba, I., Figueroa, V., Diaz-Orejas, R., & Garcia-del Portillo, F. (2015). Distinct type I and type II toxin-antitoxin modules control *Salmonella* lifestyle inside eukaryotic cells. *Scientific Reports*, *5*, 9374. https://doi.org/10.1038/srep09374

Loiseau, L., Fyfe, C., Aussel, L., Hajj Chehade, M., Hernández, S. B., Faivre, B., … Barras, F. (2017). The UbiK protein is an accessory factor necessary for bacterial ubiquinone (UQ) biosynthesis and forms a complex with the UQ biogenesis factor UbiJ. *Journal of Biological Chemistry*, *292*(28), 11937–11950. https://doi.org/10.1074/jbc.M117.789164

M9 minimal medium (standard) (2010). *Cold Spring Harbor Protocols*, 2010(8), pdb.rec12295. https://doi.org/10.1101/pdb.rec12295

Mao, C., Bhardwaj, K., Sharkady, S. M., Fish, R. I., Driscoll, T., Wower, J., … Williams, K. P. (2009). Variations on the tmRNA gene. *RNA Biology*, *6*(4), 355–361. https://doi.org/10.4161/rna.6.4.9172

Marinus, M. G., & Poteete, A. R. (2013). High efficiency generalized transduction in *Escherichia coli* O157:H7. *F1000Research*, *2*, 7. https://doi.org/10.12688/f1000research.2-7.v1

Michiels, J. E., Van den Bergh, B., Verstraeten, N., Fauvart, M., & Michiels, J. (2016). *In vitro* emergence of high persistence upon periodic aminoglycoside challenge in the ESKAPE pathogens. *Antimicrobial Agents and Chemotherapy*, *60*(8), 4630–4637. https://doi.org/10.1128/AAC.00757-16

Miller, M. H., Edberg, S. C., Mandel, L. J., Behar, C. F., & Steigbigel, N. H. (1980). Gentamicin uptake in wild-type and aminoglycoside-resistant small-colony mutants of *Staphylococcus aureus*. *Antimicrobial Agents and Chemotherapy*, *18*(5), 722–729. https://doi.org/10.1128/aac.18.5.722

Molina-Quiroz, R. C., Lazinski, D. W., Camilli, A., & Levy, S. B. (2016). Transposon-sequencing analysis unveils novel genes involved in the generation of persister cells in uropathogenic *Escherichia coli*. *Antimicrobial Agents and Chemotherapy*, *60*(11), 6907–6910. https://doi.org/10.1128/AAC.01617-16

Murphy, K. C., & Campellone, K. G. (2003). Lambda Red-mediated recombinogenic engineering of enterohemorrhagic and enteropathogenic *E. coli*. *BMC Molecular Biology*, *4*, 11. https://doi.org/10.1186/1471-2199-4-11

Nguyen, D., Joshi-Datar, A., Lepine, F., Bauerle, E., Olakanmi, O., Beer, K., … Singh, P. K. (2011). Active starvation responses mediate antibiotic tolerance in biofilms and nutrient-limited bacteria. *Science*, *334*(6058), 982–986. https://doi.org/10.1126/science.1211037

Nitzschke, A., & Bettenbrock, K. (2018). All three quinone species play distinct roles in ensuring optimal growth under aerobic and fermentative conditions in *E. coli* K12. *PLoS One*, *13*(4), e0194699. https://doi.org/10.1371/journal.pone.0194699

Norton, J. P., & Mulvey, M. A. (2012). Toxin-antitoxin systems are important for niche-specific colonization and stress resistance of uropathogenic *Escherichia coli*. *PLoS Path*, *8*(10), e1002954. https://doi.org/10.1371/journal.ppat.1002954

Pelosi, L., Ducluzeau, A. L., Loiseau, L., Barras, F., Schneider, D., Junier, I., & Pierrel, F. (2016). Evolution of ubiquinone biosynthesis: Multiple proteobacterial enzymes with various regioselectivities to catalyze three contiguous aromatic hydroxylation reactions. *mSystems*, *1*(4), e00091-16. https://doi.org/10.1128/mSystems.00091-16

Pelosi, L., Vo, C. D., Abby, S. S., Loiseau, L., Rascalou, B., Hajj Chehade, M., … Pierrel, F. (2019). Ubiquinone biosynthesis over the entire O2 range: Characterization of a conserved O2-independent pathway. *Mbio*, *10*(4), e01319-19. https://doi.org/10.1128/mBio.01319-19

Pontes, M. H., & Groisman, E. A. (2019). Slow growth determines nonheritable antibiotic resistance in *Salmonella enterica*. *Science Signalling*, *12*(592), eaax3938. https://doi.org/10.1126/scisignal.aax3938

Poon, W. W., Davis, D. E., Ha, H. T., Jonassen, T., Rather, P. N., & Clarke, C. F. (2000). Identification of *Escherichia coli ubiB*, a gene required for the first monooxygenase step in ubiquinone biosynthesis. *Journal of Bacteriology*, *182*(18), 5139–5146. https://doi.org/10.1128/jb.182.18.5139-5146.2000

Proctor, R. A., Kriegeskorte, A., Kahl, B. C., Becker, K., Löffler, B., & Peters, G. (2014). *Staphylococcus aureus* Small Colony Variants (SCVs): A road map for the metabolic pathways involved in persistent infections.

Frontiers in Cellular and Infection Microbiology, *4*, 99. https://doi.org/10.3389/fcimb.2014.00099

Ronneau, S., & Helaine, S. (2019). Clarifying the link between toxin-antitoxin modules and bacterial persistence. *Journal of Molecular Biology*, *431*(18), 3462–3471. https://doi.org/10.1016/j.jmb.2019.03.019

Schmidt, A., Kochanowski, K., Vedelaar, S., Ahrné, E., Volkmer, B., Callipo, L., … Heinemann, M. (2015). The quantitative and condition-dependent *Escherichia coli* proteome. *Nature Biotechnology*, *34*(1), 104–110. https://doi.org/10.1038/nbt.3418

Shan, Y., Brown Gandt, A., Rowe, S. E., Deisinger, J. P., Conlon, B. P., & Lewis, K. (2017). ATP-dependent persister formation in *Escherichia coli*. *Mbio*, *8*(1), e02267-16. https://doi.org/10.1128/mBio.02267-16

Shan, Y., Lazinski, D., Rowe, S., Camilli, A., & Lewis, K. (2015). Genetic basis of persister tolerance to aminoglycosides in *Escherichia coli*. *Mbio*, *6*(2), e00078-15. https://doi.org/10.1128/mBio.00078-15

Sharma, P., Teixeira de Mattos, M. J., Hellingwerf, K. J., & Bekker, M. (2012). On the function of the various quinone species in *Escherichia coli*. *FEBS Journal*, *279*(18), 3364–3373. https://doi.org/10.1111/j.1742-4658.2012.08608.x

Shen, Y., Goldsmith-Fischman, S., Atreya, H. S., Acton, T., Ma, L. C., Xiao, R., … Szyperski, T. (2005). NMR structure of the 18 kDa protein CC1736 from *Caulobacter crescentus* identifies a member of the START domain superfamily and suggests residues mediating substrate specificity. *Proteins*, *58*(3), 747–750. https://doi.org/10.1002/prot.20365

Snoussi, M., Talledo, J. P., Del Rosario, N. A., Mohammadi, S., Ha, B. Y., Kosmrlj, A., & Taheri-Araghi, S. (2018). Heterogeneous absorption of antimicrobial peptide LL37 in *Escherichia coli* cells enhances population survivability. *Elife*, *7*, e38174. https://doi.org/10.7554/eLife.38174

Søballe, B., & Poole, R. K. (2000). Ubiquinone limits oxidative stress in *Escherichia coli*. *Microbiology*, *146*(Pt 4), 787–796. https://doi.org/10.1099/00221287-146-4-787

Stefely, J. A., & Pagliarini, D. J. (2017). Biochemistry of mitochondrial coenzyme Q biosynthesis. *Trends in Biochemical Sciences*, *42*(10), 824–843. https://doi.org/10.1016/j.tibs.2017.06.008

Szklarczyk, D., Gable, A. L., Lyon, D., Junge, A., Wyder, S., Huerta-Cepas, J., … Mering, C. (2018). STRING v11: Protein-protein association networks with increased coverage, supporting functional discovery in genome-wide experimental datasets. *Nucleic Acids Research*, *47*(D1), D607–D613. https://doi.org/10.1093/nar/gky1131

Tran, U. C., & Clarke, C. F. (2007). Endogenous synthesis of coenzyme Q in eukaryotes. *Mitochondrion*, *7*(Suppl), S62–S71. https://doi.org/10.1016/j.mito.2007.03.007

Tsui, H. S., Pham, N. V. B., Amer, B. R., Bradley, M. C., Gosschalk, J. E., Gallagher-Jones, M., … Clarke, C. F. (2019). Human COQ10A and COQ10B are distinct lipid-binding START domain proteins required for coenzyme Q function. *Journal of Lipid Research*, *60*(7), 1293–1310. https://doi.org/10.1194/jlr.M093534

Van den Bergh, B., Michiels, J. E., Wenseleers, T., Windels, E. M., Boer, P. V., Kestemont, D., … Michiels, J. (2016). Frequency of antibiotic application drives rapid evolutionary adaptation of *Escherichia coli* persistence. *Nature Microbiology*, *1*, 16020. https://doi.org/10.1038/nmicrobiol.2016.20

Verstraeten, N., Knapen, W. J., Kint, C. I., Liebens, V., Van den Bergh, B., Dewachter, L., … Michiels, J. (2015). Obg and membrane depolarization are part of a microbial bet-hedging strategy that leads to antibiotic tolerance. *Molecular Cell*, *59*(1), 9–21. https://doi.org/10.1016/j.molcel.2015.05.011

Wang, Y., & Hekimi, S. (2016). Understanding ubiquinone. *Trends in Cell Biology*, *26*(5), 367–378. https://doi.org/10.1016/j.tcb.2015.12.007

White, M. D., Payne, K. A. P., Fisher, K., Marshall, S. A., Parker, D., Rattray, N. J. W., … Leys, D. (2015). UbiX is a flavin prenyltransferase required for bacterial ubiquinone biosynthesis. *Nature*, *522*(7557), 502–506. https://doi.org/10.1038/nature14559

Xia, H., Yang, X., Tang, Q., Ye, J., Wu, H., & Zhang, H. (2017). EsrE-A *yigP* locus-encoded transcript-Is a 3′ UTR sRNA involved in the respiratory chain of *E. coli*. *Frontiers in Microbiology*, *8*, 1658. https://doi.org/10.3389/fmicb.2017.01658

Yang, J. H., Bening, S. C., & Collins, J. J. (2017). Antibiotic efficacy-context matters. *Current Opinion in Microbiology*, *39*, 73–80. https://doi.org/10.1016/j.mib.2017.09.002

Zampol, M. A., Busso, C., Gomes, F., Ferreira-Junior, J. R., Tzagoloff, A., & Barros, M. H. (2010). Over-expression of COQ10 in *Saccharomyces cerevisiae* inhibits mitochondrial respiration. *Biochemical and Biophysical Research Communications*, *402*(1), 82–87. https://doi.org/10.1016/j.bbrc.2010.09.118

Zaslaver, A., Bren, A., Ronen, M., Itzkovitz, S., Kikoin, I., Shavit, S., … Alon, U. (2006). A comprehensive library of fluorescent transcriptional reporters for *Escherichia coli*. *Nature Methods*, *3*(8), 623–628. https://doi.org/10.1038/nmeth895

Zhang, Y., & Inouye, M. (2011). RatA (YfjG), an *Escherichia coli* toxin, inhibits 70S ribosome association to block translation initiation. *Molecular Microbiology*, *79*(6), 1418–1429. https://doi.org/10.1111/j.1365-2958.2010.07506.x

How to cite this article: Fino C, Vestergaard M, Ingmer H, Pierrel F, Gerdes K, Harms A, PasT of *Escherichia coli* sustains antibiotic tolerance and aerobic respiration as a bacterial homolog of mitochondrial Coq10. *MicrobiologyOpen*. 2020;00:e1064. https://doi.org/10.1002/mbo3.1064

APPENDIX 1

TABLE A1 List of all strains used in this study

Strain	Genotype	Source/description
CF323	*Escherichia coli* K-12 MG1655: F^- λ^-*ilvG*$^-$ *rfb-50 rph-1*	Wild-type strain; Gerdes laboratory collection
EG94	*E. coli* K-12 MG1655 Δ*hipAB*::FRT pBAD33 P*araB*:: SD4 *atg hipA*	MG1655 *hipAB*::FRT harboring pBAD33 P*araB*:: SD4 *atg hipA* (Germain et al., 2013)
CF083	*E. coli* K-12 MG1655 Δ*ratAB*	This study; derivative of *E. coli* K-12 MG1655 with scarless deletion of *ratAB*
CF002	*Escherichia coli* CFT073: *hly*$^+$ *pap*1$^+$ *sfa*1$^+$ *pil*1$^+$ (*rpoS*$_{am}$)	Obtained from Anders Løbner-Olesen; a 5 bp duplication (TAGAG) at the 3′ end of *c3307* ORF causes a frameshift and premature amber stop codon in *rpoS* as reported earlier (Hryckowian et al., 2015); used throughout most of this study
CF069	*E. coli* CFT073 Δ*pasTI* (*rpoS*$_{am}$)	This study; derivative of CF002 with scarless deletion of *pasTI*; used throughout most of this study
CF370	*E. coli* CFT073 (intact *rpoS*)	*E. coli* CFT073 wild-type with intact *rpoS*; obtained from Daniel R. Brown, Imperial College London (UK)
CF378	*E. coli* CFT073 Δ*pasTI* (intact *rpoS*)	This study; derivative of CF370 with scarless deletion of *pasTI*
ALO3978	*E. coli* GM9255 EDL933 (933w Δstx2AB::kan)	Anders Løbner-Olesen laboratory collection; attenuated version of *E. coli* O157:H7 strain EDL933 with deletion of the Shiga toxin (Marinus & Poteete, 2013)
CF583	EDL933 Δ*pasTI*	This study; derivative of ALO3978 with scarless deletion of *pasTI*
CF555	*E. coli* 55989	Obtained from Karen A. Krogfelt, Roskilde University (DK)
CF598	*E. coli* 55989 Δ*pasTI*::FRT	This study; derivative of CF555 after disruption of *pasTI* locus with an FRT-*km*FRT selectable cassette, then flipped out
CF557	*Salmonella enterica* serovar *enterica* str. SR-11	Obtained from Karen A. Krogfelt, Roskilde University (DK)
CF587	SR-11 Δ*pasTI*	This study; derivative of CF557 with scarless deletion of *pasTI*
CF574	*E. coli* K-12 MG1655 Δ*ubiA*::*cat*	Pierrel laboratory collection (Pelosi et al., 2019)
CF575	*E. coli* K-12 MG1655 Δ*ubiX*::*km*	Pierrel laboratory collection (Pelosi et al., 2019)

APPENDIX 2

TABLE A2 List of all plasmids used in this study

Identifier	Plasmid	Genotype/selection	Source/description/construction
n.a.	pNDM220	mini-R1 ori; *bla*; *lacI*^{q}; P*lac* promoter. Amp 30 μg/ml	Gerdes laboratory collection
n.a.	pBAD33	pA15 ori; *cat*; *araC*; P*araB* promoter. Cam 25 μg/ml	Gerdes laboratory collection
n.a.	pWRG99	TS ori; *bla*; P*araB* promoter; λred. Amp 100 μg/ml	(Blank et al., 2011); recombineering plasmid
n.a.	pKO4/pELO4	Cam 25 μg/ml	(Lee et al., 2001); template plasmid for amplification of the *cat-sacB* cassette for recombineering
n.a.	pKM208	TS ori; *bla*; P*lac* promoter; λred Amp 100 μg/ml	(Murphy & Campellone, 2003); recombineering plasmid
n.a.	pCP20	TS ori; *bla*; Amp 100 μg/ml	Gerdes laboratory collection; plasmid used to flip out the resistance cassette upon expression of the flippase (FLP) at 30°C
n.a.	pKD3	Amp 30 μg/ml; Cam 25 30 μg/ml	Gerdes laboratory collection; template plasmid for amplification of the *FRT-cat-FRT* cassette for recombineering
n.a.	pKD13	Amp 30 μg/ml; Km 25 30 μg/ml	Gerdes laboratory collection; template plasmid for amplification of the *FRT-km-FRT* cassette for recombineering
n.a.	pAH186_ColE1	ColE1 ori; *bla*; *lacI*^{q}; P*lac* promoter. Amp 100 μg/ml	This study; derivative of pNDM220 with ColE1 *ori* (copy number 15-20) instead of mini-R1; the ColE1 *ori* was amplified from pBR322 (our collection) with primers prAH1206/prAH1207, and a fragment comprising *bla-lacI*^{q}-P*lac* was amplified from pNDM220 with primers prAH1202/prAH1203; the PCR products were ligated after restriction digest with NsiI and HindIII
n.a.	pAH186_SC101	SC101 ori; *bla*; *lacI*^{q}; P*lac* promoter. Amp 100 μg/ml	This study; derivative of pNDM220 with SC101 *ori* (copy number ~5) instead of mini-R1; the SC101 *ori* was amplified from pUA139 (Zaslaver et al., 2006) with primers prAH1204/prAH1205, and a fragment comprising *bla-lacI*^{q}-P*lac* was amplified from pNDM220 with primers prAH1202/prAH1203; the PCR products were ligated after restriction digest with NsiI and HindIII
Inducible *pasT* (low copy)	pCF001_*pasT*_v$_1$	Derivative of pNDM220 encoding *pasT*. Amp 30 μg/ml	This study; the *pasT* ORF was amplified from *E. coli* CFT073 with a strong RBS and a GTG SC (AGGAGAaacaattttGTG) using primers prCF070/prCF071 and ligated into pNDM220 downstream P*lac* after digestion of backbone and insert with BamHI/EcoRI. The GTG has been converted into ATG by site-directed mutagenesis using primers prCF291/prCF292. IPTG induction of *pasT* expression.

(Continues)

TABLE A2 (Continued)

Identifier	Plasmid	Genotype/selection	Source/description/construction
Inducible *pasT* (high copy)	pAH186_ColE1_*pasT*_v_1	Derivative of pAH186_ColE1 encoding *pasT*. Amp 100 µg/ml	This study; the *pasT* ORF was amplified from *E. coli* CFT073 with a strong RBS and a GTG SC (AGGAGAaacaattttGTG) using primers prCF070/prCF071 and ligated into pAH186_ColE1 downstream P*lac* after digestion of backbone and insert with BamHI/EcoRI. The GTG has been converted into ATG by site-directed mutagenesis using primers prCF291/prCF292. IPTG induction of *pasT* expression
Inducible *pasT* (medium copy)	pAH186_SC101_*pasT*_v_1	Derivative of pAH186_SC101 encoding *pasT*. Amp 100 µg/ml	This study; the *pasT* ORF was amplified from *E. coli* CFT073 with a strong RBS and a GTG SC (AGGAGAaacaattttGTG) using primers prCF070/prCF071 and ligated into pAH186_SC101 downstream P*lac* after digestion of backbone and insert with BamHI/EcoRI. The GTG has been converted into ATG by site-directed mutagenesis using primers prCF291/prCF292. IPTG induction of *pasT* expression
pdoc	pAH154_doc_v2	Derivative of pNDM220 encoding doc. Amp 30 µg/ml	This study; the ORF of doc was amplified from bacteriophage P1vir with a weak RBS (ATTCCTCCaacaattttATG) using primers prAH1542/prAH1541 and ligated into pNDM220 downstream Plac after digestion of backbone and insert with KpnI/XhoI. IPTG induction of doc expression
ppasTI	pCF006_pasTI_v1	Derivative of pNDM220 encoding pasTI. Amp 30 µg/ml	This study; pasTI operon including ≈300 bp upstream was amplified from *E. coli* CFT073 using primers prCF222/prCF223 and ligated into pNDM220 after digestion of backbone and insert with BamHI/EcoRI. V1 = strong SD and original SC (ATG). Expression of pasTI under endogenous transcriptional control
pratAB	pCF006_ratAB_v1	Derivative of pNDM220 encoding ratAB. Amp 30 µg/ml	This study; ratAB operon including ≈300 bp upstream was amplified from *E. coli* MG1655 using primers prCF222/prCF224 and ligated into pNDM220 after digestion of backbone and insert with BamHI/EcoRI. V1 = strong SD and original SC (ATG). Expression of ratAB under endogenous transcriptional control
ppasT	pCF006_pasT_v1	Derivative of ppasTI (pCF006_pasTI_v1) encoding only pasT. Amp 30 µg/ml	This study; pasI ORF was deleted from ppasTI by site-directed mutagenesis using primers prCF236/prCF237
pratA	pCF006_ratA_v1	Derivative of pratAB (pCF006_ratAB_v1) encoding only ratA. Amp 30 µg/ml	This study; ratB ORF was deleted from pratAB by site-directed mutagenesis using primers prCF236/prCF240
pratB	pCF006_ratB_v1	Derivative of pratAB (pCF006_ratAB_v1) encoding only ratB. Amp 30 µg/ml	This study; ratA ORF was deleted from pratAB by site-directed mutagenesis using primers prCF238/prCF239

(Continues)

TABLE A2 (Continued)

Identifier	Plasmid	Genotype/selection	Source/description/construction
pCC1736	pCF007_cc1736_v1	Derivative of pNDM220 encoding cc1736. Amp 30 μg/ml	This study; codon-optimized cc1736 ORF was synthesized by GenScript, amplified using primers prCF256/prCF257, and ligated into pNDM220 downstream of Plac after digestion of backbone and insert with BamHI/XhoI digestion. V1 = strong RBS and original start codon (CTG). IPTG induction of cc1736 expression
pCOQ10	pCF007_coq10_v4	Derivative of pNDM220 encoding coq10A. Amp 30 μg/ml	This study; codon-optimized coq10 ORF (isoform A) was synthesized by GenScript, amplified using primers prCF259/prCF290, and ligated into pNDM220 downstream Plac after digestion of backbone and insert with BamHI/XhoI. V4 = N-terminus truncated variant. IPTG induction of coq10A expression
ppasI	pCF003_pasI_v1	Derivative of pBAD33 encoding pasI. Cam 25 μg/ml	This study; pasI ORF was amplified from *E. coli* CFT073 with a strong RBS and a GTG SC (AGGAGAaacaattttGTG) using primers prCF166/prCF251 and ligated into pBAD33 downstream ParaB after digestion of backbone and insert with HindIII/XbaI. Arabinose induction of pasI expression. V1 = original SC (GTG) and strong RBS
phipA	pBAD33 ParaB:: SD4 atg hipA	Derivative of pBAD33 encoding hipA. Cam 25 μg/ml	Gerdes laboratory collection. hipA ORF was amplified from *E. coli* K-12 MG1655 with a strong RBS and an ATG SC (AAGGAaaaaATG) using primers OEG89/OEG60 (Germain et al., 2013) and ligated into pBAD33 downstream ParaB promoter after digestion of backbone and insert with XbaI/SphI. Arabinose induction of hipA expression

Abbreviations: Amp, Ampicillin; *araC*, encodes the regulator of P*araB*; *bla*, β-lactamase-encoding cassette; Cam, Chloramphenicol; *cat*, Chloramphenicol acetyltransferase; IPTG, Isopropyl β-D-1-thiogalactopyranoside; Kan, Kanamycin; $lacI^q$, encodes the repressor of P*lac* (allele with strong *lacI* expression); ori, plasmid origin of replication; P*araB*, promoter inducible with L-arabinose; P*lac*, Promoter inducible with IPTG; RBS, Ribosome binding site; SC, Start codon; TS, temperature-sensitive; λ*red*, recombineering system.

TABLE A3 Oligonucleotides used in this study

Oligo name	Sequence	Description
pasTI/ratAB deletion		
prCF025	GTGCTCAATGAGCACCTTTTTTCTGTCTGTTATTTATTCGCTGATTTTTCCTGGTGTC CCTGTTGATACC	rv. MG1655/CFT073. Amplification of *cat-sacB* cassette. Homology to the cassette is highlighted
prCF026	CCGATGTTACCCAGCGCCGGGATAGCGTTTTTTTTACAGCAGGATAAATGGGAAAA CTGTCCATATGCAC	fw. MG1655/CFT073. Amplification of *cat-sacB* cassette; Homology to the cassette is highlighted
prCF027	AGCACCTTTTTTCTGTCTGTTATTTATTCGCTGATTTTTCCATTTATCCTGCTGTAAAA AAAACGCTATCCCGGCGCTGG	rv. MG1655/CFT073. Scarless deletion of the *cat-sacB* cassette
prCF028	CCAGCGCCGGGATAGCGTTTTTTTTACAGCAGGATAAATGGAAAAATCAGCGAAT AAATAACAGACAGAAAAAAGGTGCT	fw. MG1655/CFT073. Scarless deletion of the *cat-sacB* cassette
prCF323	GTGCTCAATGAGCACCTTTTTTTCTGTCCGTTATTTATTCGCTGATTTTTCCTGGTGTC CCTGTTGATACC	rv. EDL933. Amplification of *cat-sacB* cassette. Homology to the cassette is highlighted
prCF324	GGATGTTACCCAGCGCCGGGATAGCGTTTTTTTTACTGCAGGATAAATGGGAAAAC TGTCCATATGCAC	fw. EDL933. Amplification of *cat-sacB* cassette. Homology to the cassette is highlighted
prCF325	AGCACCTTTTTTCTGTCCGTTATTTATTCGCTGATTTTTCCATTTATCCTGCAGTAAA AAAAACGCTATCCCGGCGCTGG	rv. EDL933. Scarless deletion of the *cat-sacB* cassette
prCF326	CCAGCGCCGGGATAGCGTTTTTTTTACTGCAGGATAAATGGAAAAATCAGCGAATA AATAACGGACAGAAAAAAGGTGCT	fw. EDL933. Scarless deletion of the *cat-sacB* cassette
prCF329	CCACACCGTTATCCGGCAAAAGAGGCTAATTATCTGCCAGCCGATTTTTCCTGGTGT CCCTGTTGATACC	rv. SR11. Amplification of *cat-sacB* cassette. Homology to the cassette is highlighted
prCF330	ATTAAGGCATGACGGTTGGGGACAGCATTTTTTTTACTCGCTGATAAGTGGGAAAA CTGTCCATATGCAC	fw. SR11. Amplification of *cat-sacB* cassette. Homology to the cassette is highlighted
prCF331	ATCCGGCAAAAGAGGCTAATTATCTGCCAGCCGATTTTTCCACTTATCAGCGAGTA AAAAAAATGCTGTCCCCAACCGTC	rv. SR11. Scarless deletion of the *cat-sacB* cassette
prCF332	GACGGTTGGGGACAGCATTTTTTTTACTCGCTGATAAGTGGAAAAATCGGCTGGCA GATAATTAGCCTCTTTTGCCGGAT	fw. SR11. Scarless deletion of the *cat-sacB* cassette
prCF231	GTGCTCAATGAGCACCTTTTTTTCTGTCTGTTATTTATTCGCTGATTTTTCTGTAGGCT GGAGCTGCTTCG	rv. 55989. Amplification of FRT-*km*-FRT cassette. Homology to the cassette is highlighted
prCF232	CCGATGTTACCCAGCGCCGGGATAGCGTTTTTTTTACAGCAGGATAAATGATTCCG GGGATCCGTCGACC	fw. 55989. Amplification of FRT-*km*-FRT cassette. Homology to the cassette is highlighted
prCF023	GAACTATCTGACCGCTAACGAC	rv. Screening *pasTI/ratAB* locus
prCF024	GTCGCGCAGAAGGAC	fw. Screening *pasTI* locus
prCF033	GAAATGCCTCTCCGTCAC	fw. Screening *ratAB* locus and *pasTI* locus of 55989
prCF327	GGAACTATCTTACACCTACGGAT	rv. SR11. Screening *pasTI* locus
prCF328	CGCCATCTTTGAGGATAAC	fw. SR11. Screening *pasTI* locus
pCF001_*pasT*_v$_1$ construction and related plasmids		
prCF070	CCCGAGGGATCCAGGAGAAACAATTTTGTGATATTATTTGTTGGATTTTTGTTG	fw. Amplification of *pasT* gene. BamHI RS
prCF071	GGGCTCGAATTCTTACCTGGCACTGTAGACCTC	rv. Amplification of *pasT* gene. EcoRI RS
prCF291	ACAATTTTATGATATTATTTGTTGGATTTTTGTTG	fw. GTG to ATG conversion
prCF292	TAATATCATAAAATTGTTTCTCCTGGATCC	rv; GTG to ATG conversion

(Continues)

TABLE A3 (Continued)

Oligo name	Sequence	Description
pCF006_*pasTI*_v_1 and pCF006_*ratAB*_v_1 construction		
prCF222	ACCGAGGGATCCAGGAGAAACAATTTTGGACATAGCTGTCGCTGATA	fw. Amplification of *pasTI* operon. BamHI RS
prCF223	GGGCTCGAATTCTTATTTATTCGCTGATTTTTCTG	rv. Amplification of *pasTI/ratAB* operon. EcorI RS
prCF224	ACCGAGGGATCCAGGAGAAACAATTTTGGACGTAGCTGTCGCTG	fw. Amplification of ratAB operon. BamHI RS
pCF006_*pasT*_v_1 and pCF006_*ratA*_v_1 construction		
prCF236	TGCCAGGTAAGAATTCACTGGCCGTCG	fw. Deletion of *pasI/ratB* from pCF006_*pasTI/ratAB*_v_1
prCF237	AGTGAATTCTTACCTGGCACTGTAGACCTC	rv. Deletion of *pasI* from pCF006_*pasTI*_v_1
prCF240	AGTGAATTCTTACCTGGCACTGTAAACCTC	rv. Deletion of ratB from pCF006_ratAB_v1
pCF006_*ratB*_v_1 construction		
prCF238	AGCAGGATAAGTGCCAGGTAAAATTGCC	fw. Deletion of *ratA* from pCF006_*ratAB*_v_1
prCF239	TACCTGGCACTTATCCTGCTGTAAAAAAAACG	rv. Deletion of *ratA* from pCF006_*ratAB*_v_1
pCF003_*pasI*_v_1 construction		
prCF166	GGGCTGAAGCTTTTATTTATTCGCTGATTTTTCTG	rv. Amplification of *pasI*. HindIII RS
prCF251	CCCGAGTCTAGAAGGAGAAACAATTTTGTGCCAGGTAAAATTGCC	fw. Amplification of *pasI*. XbaI RS
pCF007_*cc1736*_v_1 construction		
prCF256	CCCGAGGGATCCAGGAGAAACAATTTTCTGCACCGTCACGTGG	fw. Amplification of *cc1736*. BamHI RS
prCF257	GGGCTCCTCGAGTTACGCACCATGCAGTTG	rv. Amplification of *cc1736*. XhoI RS
pCF007_*coq10*_v_4 construction		
prCF259	GGGCTCCTCGAGTTAGGTTTGGTGAACTTCGT	rv. Amplification of *coq10A*. XhoI RS
prCF290	CAAGAGGGATCCAGGAGAAACAATTTTATGGCGTACAGCGAGCGT	fw. Amplification of *coq10A*. BamHI RS
Others		
prAH_ pNDM220	AAAACAGGAAGGCAAAATGC	fw. Screening for cloning in pNDM220
prAH500	CTGTTTTATCAGACCGCTTC	Rv. Screening for cloning in pNDM220 and pBAD33
prAH501	CGTCACACTTTGCTATGCC	fw. Screening for cloning in pBAD33
prCF262	GTTGTTTATGCCGGTAACG	fw. *rpoS* sequencing
prCF263	CAATTACTGTGCGCTTAAAATG	rv. *rpoS* sequencing
prAH1541	GCCTTCCCTCGAGCTACTCCGCAGAACCATACAA	rv. Amplification of *doc* from phage P1*vir*. XhoI RS
prAH1542	CGAGTGGGTACCATTCCTCCAACAATTTTATGAGGCATATATCACCGGA	fw. Amplification of *doc* from phage P1*vir*. KpnI RS
prAH1202	GACGCCAAGCTTCCTAGATCCTTTTAAATTAAAAATGAAG	fw. pNDM220 for pAH186 series
prAH1203	CTCCCGGATGCATGAAGCATAAAGTGTAAAGCCTG	rv. pNDM220 for pAH186 series
prAH1204	GACGCCATGCATCCGCTGTAACAAGTTGTCTC	fw. SC101 for pAH186 series
prAH1205	CTCCCGGAAGCTTCGCTTGGACTCCTGTTG	rv. SC101 for pAH186 series
prAH1206	GAGCGGATGCATAGTGATTTTTCTCTGGTCCC	fw. ColE1 for pAH186 series
prAH1207	CTCCGCCAAGCTTCCCGTAGAAAAGATCAAAGG	rv. ColE1 for pAH186 series
prAH1805	GGTTGTCTGCAGCATAAAGTGTAAAGCCTGGGG	rv. pNDM220 inserts into pAH160-P*lac*

Abbreviations: fw, Forward primer; rv, Reverse primer.

TABLE A4 Genomes used for the synteny analysis of Figure 3

Organism	Strain	GenBank/RefSeq accession number
Escherichia coli	str. K-12; substr. MG1655	**U00096.3**/NC_000913.3
Escherichia coli	str. CFT073	**AE014075.1**/NC_004431.1
Escherichia coli	str. B; substr. REL606/ Bc251	**CP000819.1**/NC_012967.1
Escherichia coli	str. UTI89	**CP000243.1**/NC_007946.1
Shigella flexneri	serotype 5a str. M90T	**CM001474.1**/NZ_CM001474.1
Salmonella enterica	subsp. *enterica*; serovar Typhimurium; str. CT18	**AL513382.1**/NC_003198.1
Pseudomonas aeruginosa	str. PAO1	**AE004091.2**/NC_002516.2
Burkholderia cenocepacia	str. J2315	Chromosome 1: **AM747720.1**/ NC_011000.1 Chromosome 2: **AM747721.1**/ NC_011001.1
Neisseria meningitidis	serogroup B; str. MC58	**AE002098.2**/NC_003112.2
Caulobacter crescentus	str. CB15/ATCC 19089	**AE005673.1**/NC_002696.2
Myxococcus xanthus	str. DK 1622	**CP000113.1**/NC_008095.1

(a) Ectopic expression of *pasT* in *E. coli* CFT073 Δ*pasTI*

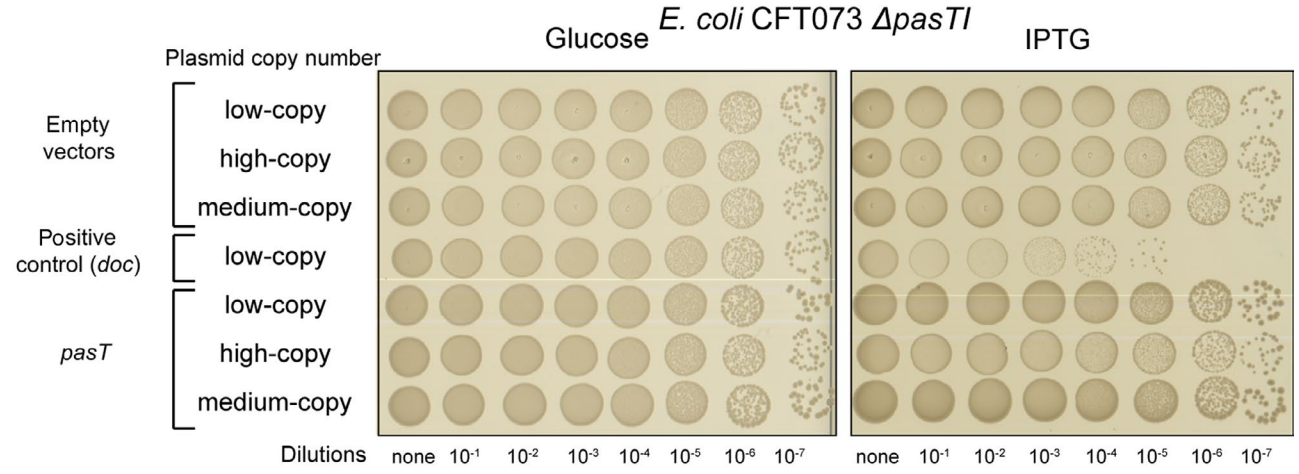

(b) Ectopic expression of *pasT* in *E. coli* K-12 MG1655 wildtype and Δ*ratAB*

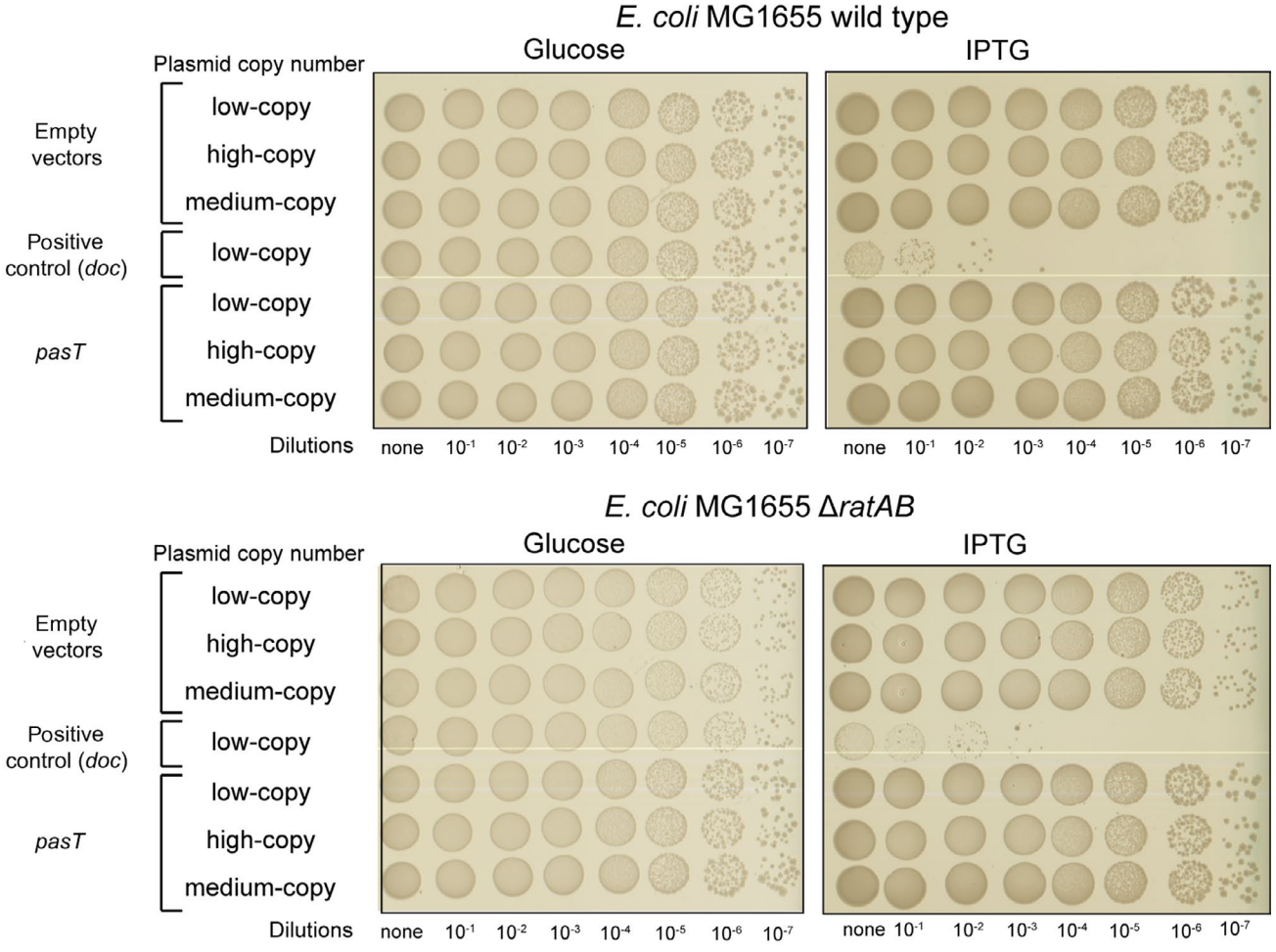

(c) Ectopic expression of *pasI* in *E. coli* K-12 MG1655 Δ*ratAB*

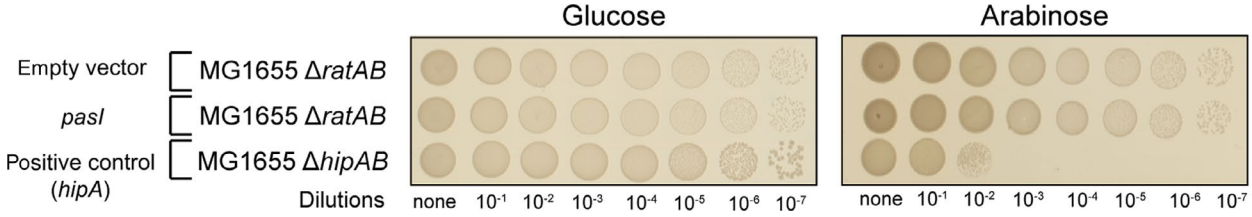

FIGURE A1 No growth inhibition is observed upon expression of *pasT* (and *pasI*) under different conditions. (a) Spot assay of *E. coli* CFT073 Δ*pasTI* mutant harboring isogenic plasmids with different copy number encoding either *pasT* or the well-studied TA module toxin *doc* (as positive control) under control of a P*lac* promoter induced on LB agar plates containing 1 mM isopropyl β-D-1-thiogalactopyranoside (IPTG) and repressed on LB agar plates containing 1% w/v D-glucose (see Materials and Methods). The expression of *pasT* did not cause growth inhibition under any condition. (b) The same experiment as shown in (a) for *E. coli* CFT073 *ΔpasTI* was performed with *E. coli* K-12 MG1655 wild-type (top)/Δ*ratAB* (bottom). No growth inhibition was detected for *pasT* expression under any condition. (c) Spot assay of *E. coli* K-12 MG1655 Δ*ratAB* harboring a plasmid encoding either *pasI* or the well-studied TA module toxin *hipA* (as positive control) under control of a P*araB* promoter induced on agar plates containing 0.2% w/v L-arabinose and repressed on agar plates containing 1% w/v D-glucose (see Materials and Methods). No growth inhibition was detected for *pasI* expression

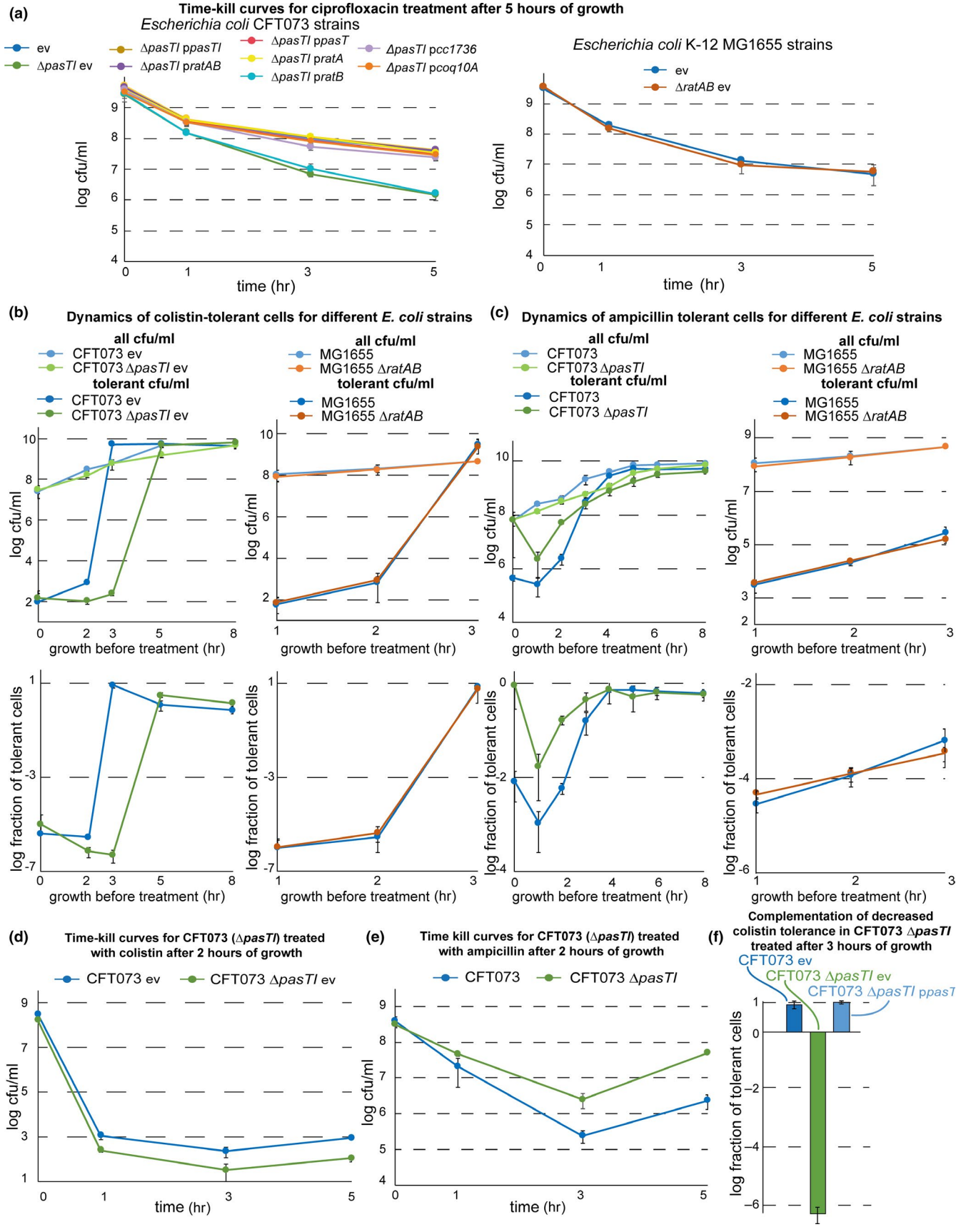
(a)
Time-kill curves for ciprofloxacin treatment after 5 hours of growth
Escherichia coli CFT073 strains
ev
ΔpasTI ev
ΔpasTI ppasTI
ΔpasTI pratAB
ΔpasTI ppasT
ΔpasTI pratA
ΔpasTI pratB
ΔpasTI pcc1736
ΔpasTI pcoq10A
log cfu/ml
time (hr)
Escherichia coli K-12 MG1655 strains
ev
ΔratAB ev
log cfu/ml
time (hr)
(b)
Dynamics of colistin-tolerant cells for different E. coli strains
all cfu/ml
CFT073 ev
CFT073 ΔpasTI ev
tolerant cfu/ml
CFT073 ev
CFT073 ΔpasTI ev
all cfu/ml
MG1655
MG1655 ΔratAB
tolerant cfu/ml
MG1655
MG1655 ΔratAB
log cfu/ml
growth before treatment (hr)
log fraction of tolerant cells
growth before treatment (hr)
(c)
Dynamics of ampicillin tolerant cells for different E. coli strains
all cfu/ml
CFT073
CFT073 ΔpasTI
tolerant cfu/ml
CFT073
CFT073 ΔpasTI
all cfu/ml
MG1655
MG1655 ΔratAB
tolerant cfu/ml
MG1655
MG1655 ΔratAB
log cfu/ml
growth before treatment (hr)
log fraction of tolerant cells
growth before treatment (hr)
(d)
Time-kill curves for CFT073 (ΔpasTI) treated with colistin after 2 hours of growth
CFT073 ev
CFT073 ΔpasTI ev
log cfu/ml
time (hr)
(e)
Time kill curves for CFT073 (ΔpasTI) treated with ampicillin after 2 hours of growth
CFT073
CFT073 ΔpasTI
log cfu/ml
time (hr)
(f)
Complementation of decreased colistin tolerance in CFT073 ΔpasTI treated after 3 hours of growth
CFT073 ev
CFT073 ΔpasTI ev
CFT073 ΔpasTI ppasT
log fraction of tolerant cells

FIGURE A2 Biphasic time–kill curves reveal differences in persister levels between *E. coli* CFT073 and the Δ*pasTI* mutant. (a) The figure shows the time–kill curves of *E. coli* CFT073 (left) and *E. coli* K-12 MG1655 (right) strains treated with 10 μg/ml ciprofloxacin 5 hr after inoculation into fresh medium (see Materials and Methods). (b) The same experiment as presented in Figure 2a,b for the dynamics of ciprofloxacin-tolerant cells was repeated for treatment with 6.6 μg/ml colistin, revealing lower survival of *E. coli* CFT073 Δ*pasTI* (but not/K12 MG1655 Δ*ratAB*) during exponential growth when compared to the parental wild-type. Note that all strains seem to exhibit some resistance to colistin when the cultures reach high densities (i.e., later than the time points where differences between CFT073 wild-type and Δ*pasTI* become apparent). We suggest that this phenomenon might be caused by the heterogeneous absorption of colistin in a way that a subpopulation of nongrowing cells sequesters enough drug to enable residual growth of other cells during the treatment period (as shown before for antimicrobial peptide LL37 by Snoussi et al. (2018)). (c) The same experiment as presented in Figure 2a,b for the dynamics of ciprofloxacin-tolerant cells was repeated for treatment with 100 μg/ml ampicillin (as previously reported for Δ*pasTI* and Δ*ratAB* mutants by Norton and Mulvey (2012)). (d) The figure shows time–kill curves of *E. coli* CFT073 strains treated with 6.6 μg/ml colistin after 2 hr of growth, that is, before any of the cultures have reached high densities. (e) The figure shows time–kill curves of *E. coli* CFT073 strains treated with 100 μg/ml ampicillin after 2 hr of growth, that is, at the minimal survival observed for both wild-type and Δ*pasTI* mutant (see (c)). The regrowth observed after 3 hr in similar ways for both strains is likely due to the high intrinsic resistance of *E. coli* CFT073 to β-lactams. (f) The complementation of decreased colistin survival of *E. coli* CFT073 Δ*pasTI* was confirmed by comparing the mutant strain carrying an empty vector with an isogenic strain harboring a plasmid encoding *pasT* for complementation. All data points in (a-f) represent the mean of results from at least three independent experiments, and error bars indicate standard deviations. ev = empty vector (pNDM220)

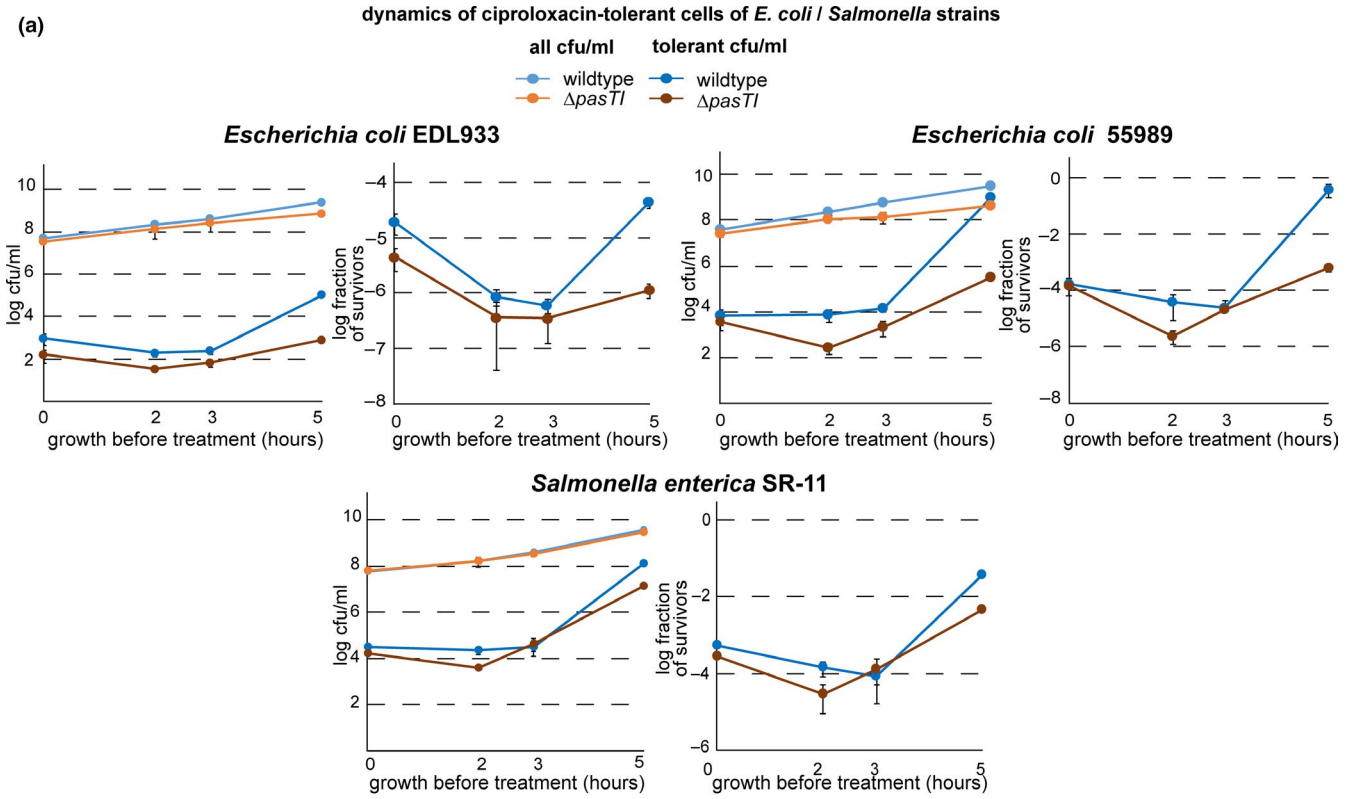
(a)
dynamics of ciproloxacin-tolerant cells of E. coli / Salmonella strains
all cfu/ml
tolerant cfu/ml
wildtype
ΔpasTI
wildtype
ΔpasTI
Escherichia coli EDL933
Escherichia coli 55989
log cfu/ml
log fraction of survivors
growth before treatment (hours)
Salmonella enterica SR-11

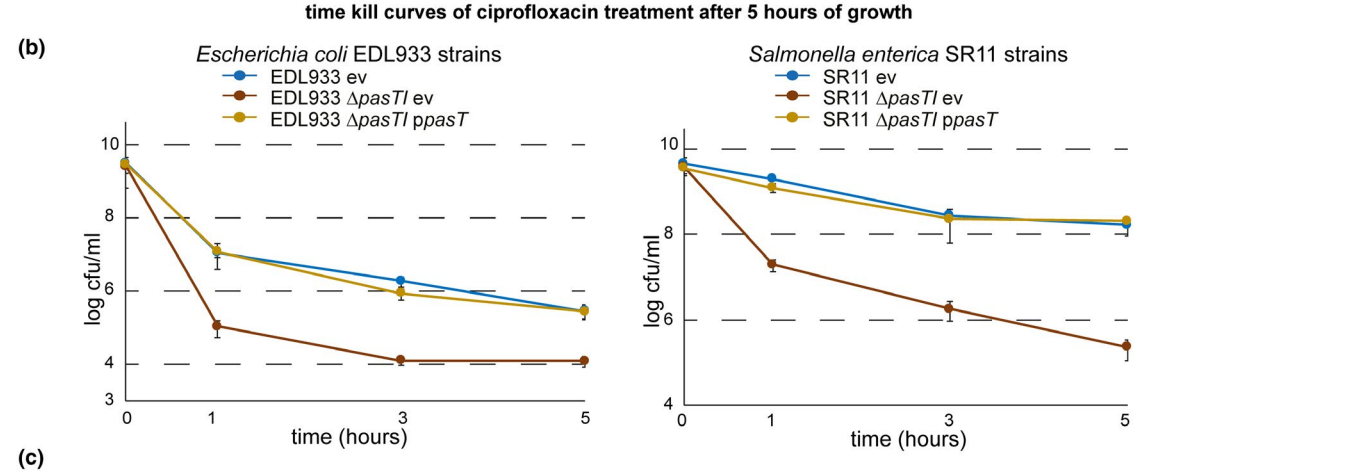
time kill curves of ciprofloxacin treatment after 5 hours of growth
(b)
Escherichia coli EDL933 strains
EDL933 ev
EDL933 ΔpasTI ev
EDL933 ΔpasTI ppasT
Salmonella enterica SR11 strains
SR11 ev
SR11 ΔpasTI ev
SR11 ΔpasTI ppasT
log cfu/ml
time (hours)

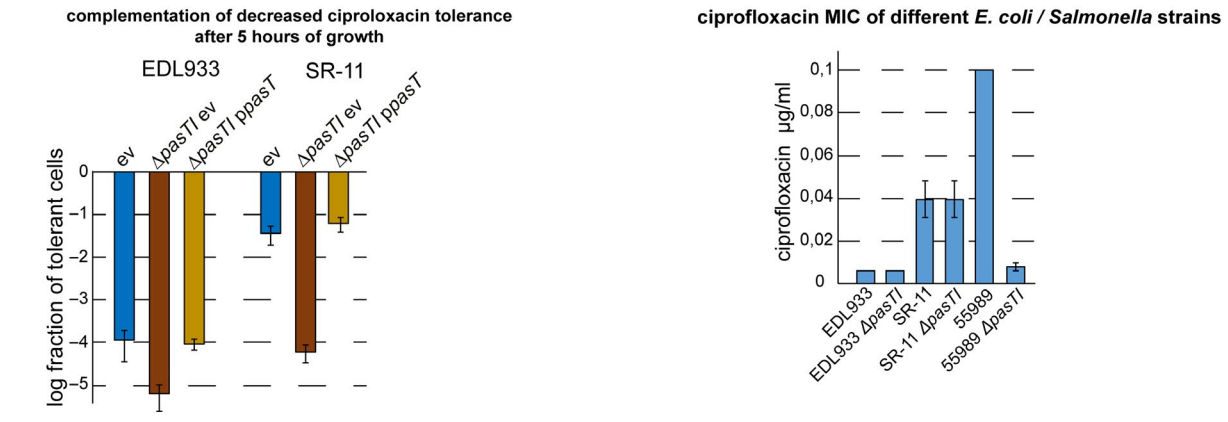
(c)
complementation of decreased ciproloxacin tolerance after 5 hours of growth
EDL933
SR-11
ev
ΔpasTI ev
ΔpasTI ppasT
log fraction of tolerant cells
ciprofloxacin MIC of different E. coli / Salmonella strains
ciprofloxacin µg/ml
EDL933
EDL933 ΔpasTI
SR-11
SR-11 ΔpasTI
55989
55989 ΔpasTI

FIGURE A3 Differences in persister levels are observed between wild-type and Δ*pasTI* variants of other *E. coli/Salmonella* strains. (a) The same experiment as presented in Figure 2a-d for the dynamics of *E. coli* CFT073 ciprofloxacin-tolerant cells was repeated for *E. coli* O157:H7 EDL933 (top left), *E. coli* 55989 (top right), and *Salmonella enterica* SR-11 (bottom). (b, c) Time–kill curves for *E. coli* EDL933 and *S. enterica* SR-11 strains treated with 10 μg/ml ciprofloxacin 5 hr after inoculation into fresh medium reveal that the antibiotic tolerance defect of *pasTI* mutants can be complemented by ectopic expression of CFT073 *pasT*. We note that there are quantitative differences in the results of seemingly similar experiments in (a) and (b) like, for example, the extent of ciprofloxacin sensitivity of the *S. enterica* SR-11 Δ*pasTI* mutant. These do not qualitatively affect the phenotypes or overall conclusions and are caused by the presence of plasmids (empty vector or complementation plasmid) in (b), while strains in (a) harbor no plasmid (see also Figure A6c,d for another phenotype affected by plasmid carriage). (d) The *pasTI* knockout did not affect the ciprofloxacin MIC of any strain except *E. coli* 55989 where it greatly reduced intrinsic ciprofloxacin resistance. It is therefore possible that for this strain (but not the others) at least part of the different survival between wild-type and *pasTI* knockout can be explained by a difference in MIC. All data points in (a-d) represent the mean of results from at least three independent experiments, and error bars indicate standard deviations. *ev* = empty vector

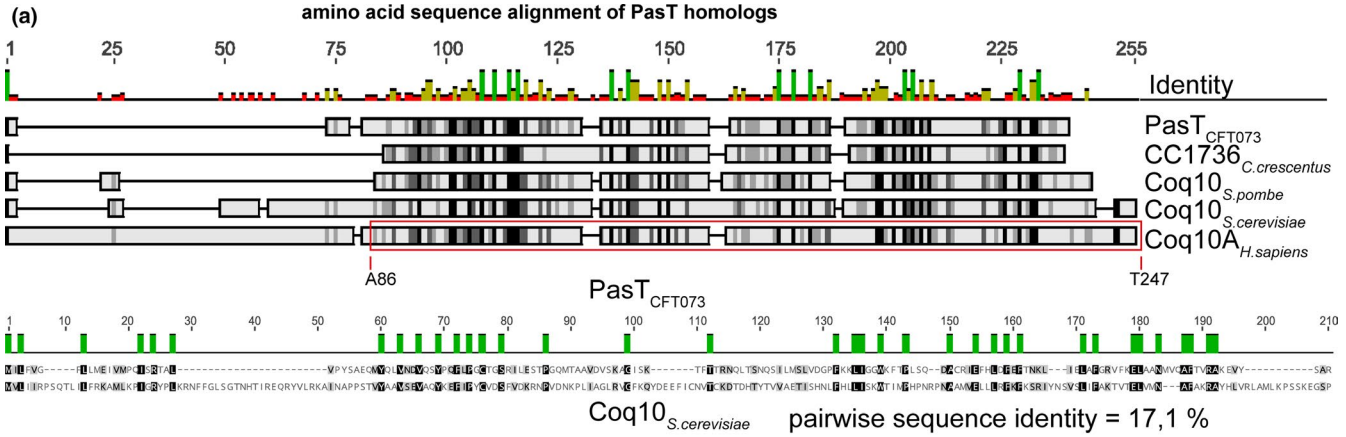

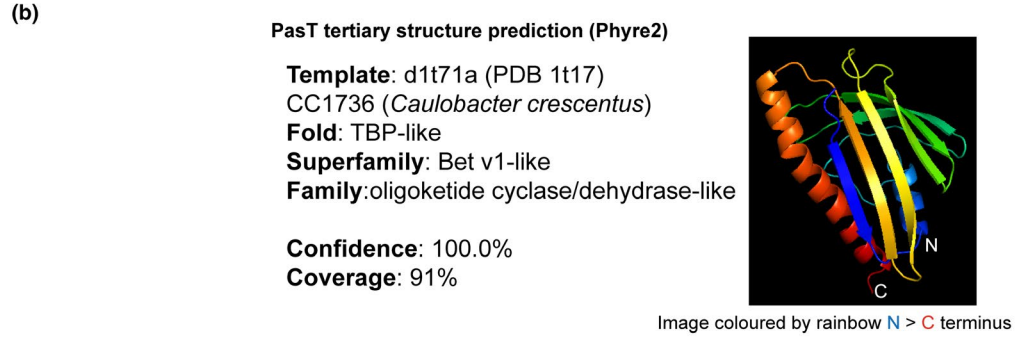

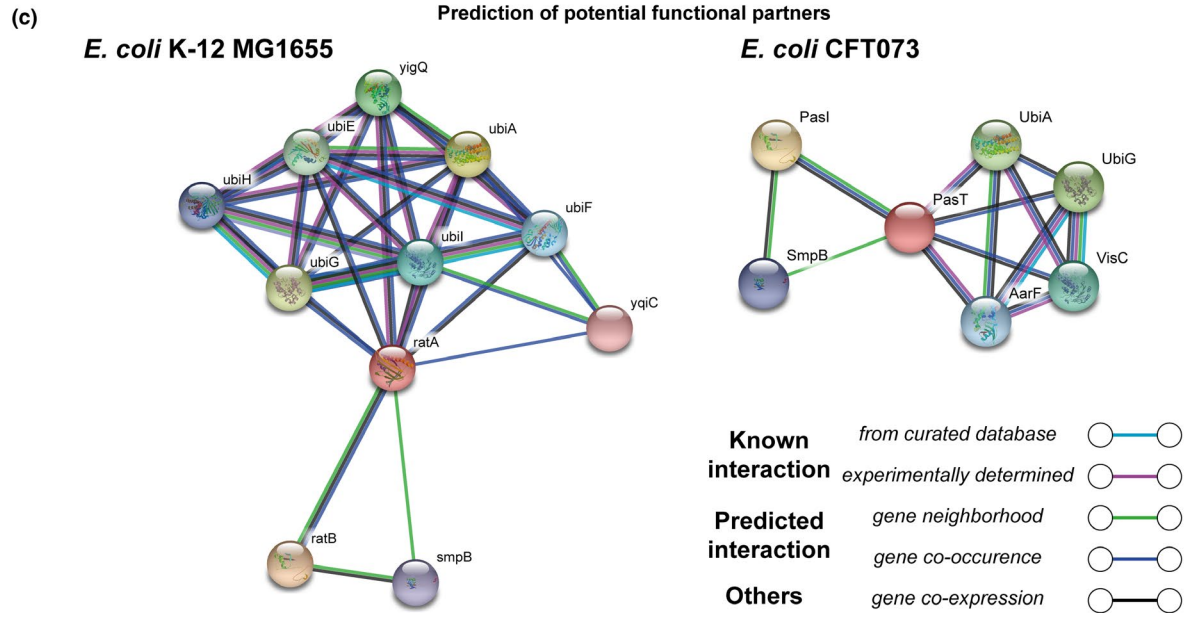

FIGURE A4 In silico analysis of relationships between PasT/RatA and Coq10 homologs. (a) The illustration shows a protein sequence alignment of different PasT homologs (generated as described in Materials and Methods). For complementation experiments (e.g., in Figure 8), we cloned the C-terminus of Coq10A that is homologous to CC1736/PasT (highlighted by a red frame; the first and the last amino acids are indicated) without the N-terminal mitochondrial targeting sequence. For completeness, a detailed amino acid sequence alignment of $PasT_{CFT073}$ and $Coq10_{S.cerevisiae}$ is provided. (b) PasT structure prediction using Phyre2 (https://www.sbg.bio.ic.ac.uk/phyre2; Kelley et al., 2015). The structure of *E. coli* CFT073 PasT was modeled with Phyre2 using the best-matching template PDB entry 1t17 (CC1736 of *Caulobacter crescentus*—see also Figure 3 and (a)—and assigned a 100% confidence. The N-terminus and C-terminus are indicated by white letters. (c) Interaction partners of *E. coli* K-12 MG1655 RatA (left) and *E. coli* CFT073 PasT (right) were analyzed using STRING (https://string-db.org/; Szklarczyk et al., 2018).

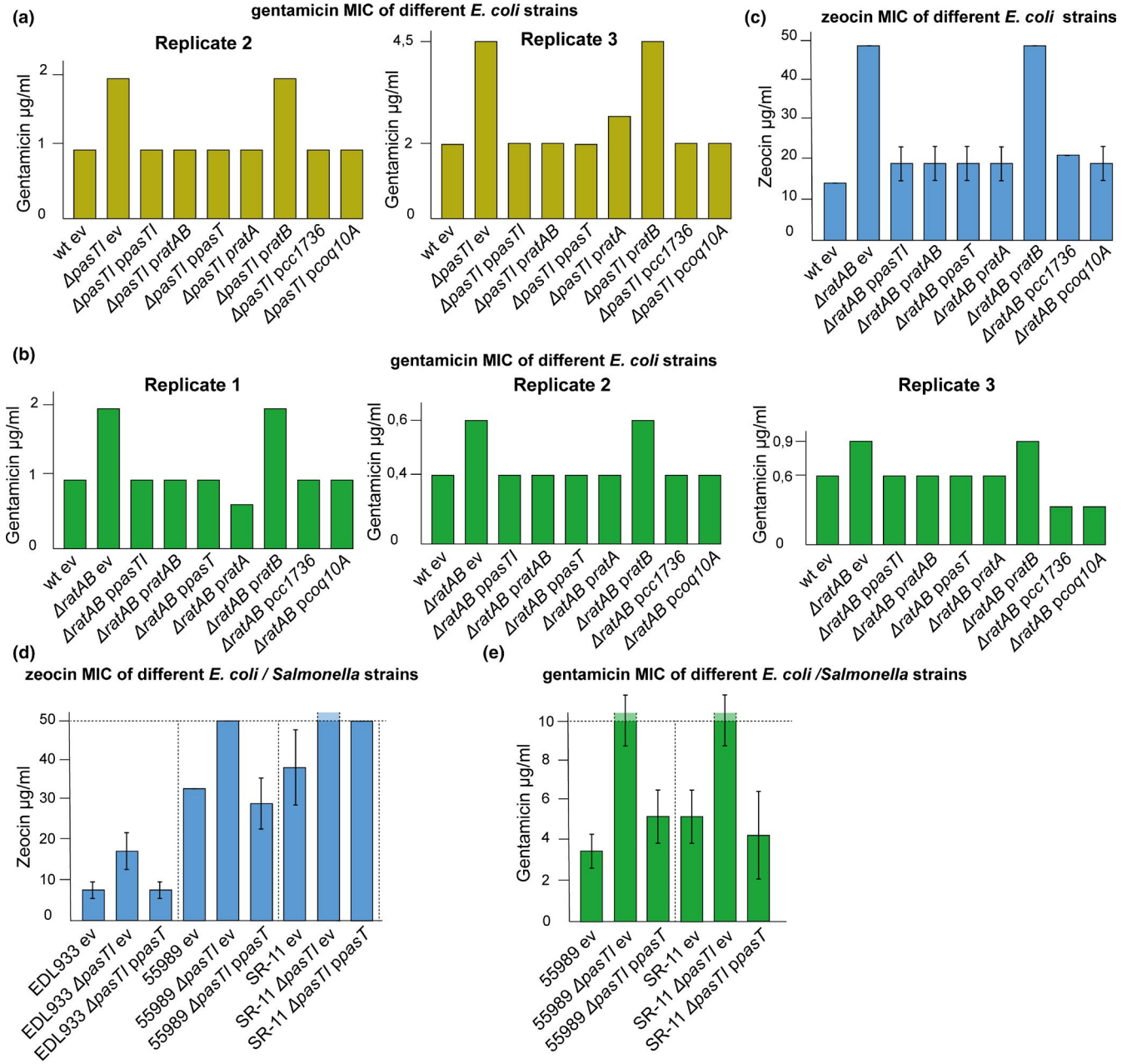

FIGURE A5 Additional data related to gentamicin and zeocin MIC experiments. (a) Two additional independent replicates of the gentamicin MIC determination for *E. coli* CFT073 strains are shown that confirm the phenotype indicated in Figure 4c, Figure 4d, and Figure 8b. (b, c) The experiments shown in Figure 4c, Figure 4d, Figure 8b, and (a) were also performed with *E. coli* K-12 MG1655 strains instead of *E. coli* CFT073 strains, revealing the same phenotypes of increased gentamicin/zeocin MIC in the absence of functional *ratA* without functional complementation by a homolog. For zeocin, data points represent the mean of results from three independent experiments, and error bars indicate standard deviations. (d, e) The MICs of *E. coli* O157:H7 EDL933, *E. coli* 55989, and *S. enterica* SR-11 and their Δ*pasTI* derivatives for gentamicin (d) and zeocin (e) were determined by broth dilution assays. The bacteria carried either an empty vector (ev) or the complementation plasmid encoding *pasT*. We did not use the EDL933 strain in (e) because of problems with gentamicin resistance. Data points in (d) and (e) represent the mean of results from at least three independent experiments, and error bars indicate standard deviation.

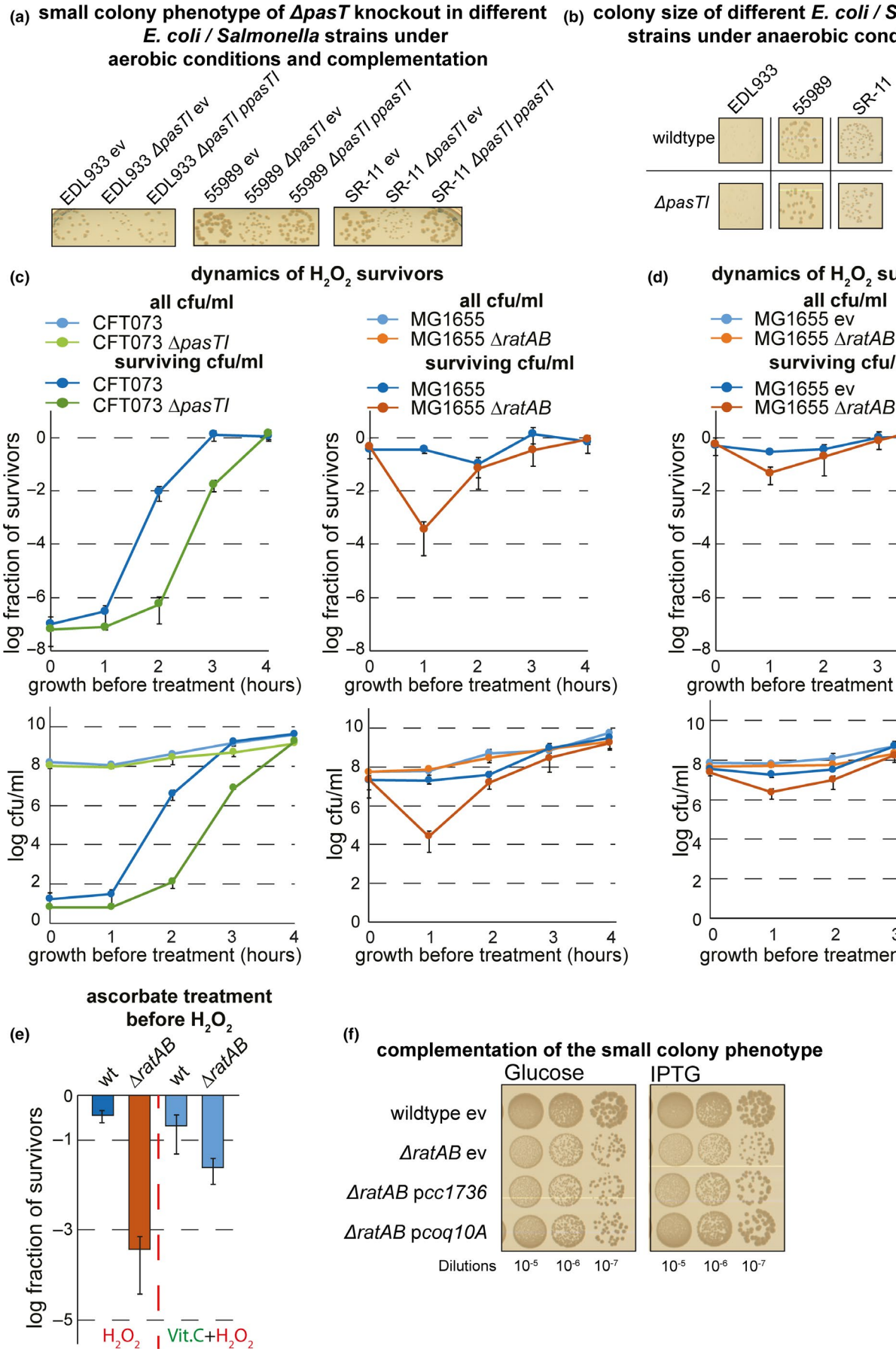
(a) small colony phenotype of ΔpasT knockout in different E. coli / Salmonella strains under aerobic conditions and complementation
EDL933 ev
EDL933 ΔpasTI ev
EDL933 ΔpasTI ppasTI
55989 ev
55989 ΔpasTI ev
55989 ΔpasTI ppasTI
SR-11 ev
SR-11 ΔpasTI ev
SR-11 ΔpasTI ppasTI
(b) colony size of different E. coli / Salmonella strains under anaerobic conditions
EDL933
55989
SR-11
wildtype
ΔpasTI
(c) dynamics of H2O2 survivors
all cfu/ml
CFT073
CFT073 ΔpasTI
surviving cfu/ml
CFT073
CFT073 ΔpasTI
log fraction of survivors
log cfu/ml
growth before treatment (hours)
all cfu/ml
MG1655
MG1655 ΔratAB
surviving cfu/ml
MG1655
MG1655 ΔratAB
(d) dynamics of H2O2 survivors
all cfu/ml
MG1655 ev
MG1655 ΔratAB ev
surviving cfu/ml
MG1655 ev
MG1655 ΔratAB ev
(e) ascorbate treatment before H2O2
wt
ΔratAB
wt
ΔratAB
H2O2
Vit.C+H2O2
(f) complementation of the small colony phenotype
Glucose
IPTG
wildtype ev
ΔratAB ev
ΔratAB pcc1736
ΔratAB pcoq10A
Dilutions
10-5
10-6
10-7

FIGURE A6 Additional data related to experiments assessing oxidative stress sensitivity. (a) *E. coli* O157:H7 EDL933, *E. coli* 55989, *S. enterica* SR-11, and their Δ*pasTI* derivatives carrying either the empty vector (ev) or the complementation plasmid (p*pasT*) were spotted on LB agar plates to visualize differences in colony size. (b) Cultures of *E. coli* O157:H7 EDL933, *E. coli* 55989, *S. enterica* SR-11, and their Δ*pasTI* derivatives were diluted and spotted on LB agar plates which we thereafter incubated in the absence of oxygen. D-glucose (1% w/v) was added as a fermentable carbon source to LB agar plates incubated anaerobically. (c) Bacterial growth (colony-forming units (cfu)/ml) and dynamics of cells surviving hydrogen peroxide (H_2O_2) treatment were determined for cultures of *E. coli* CFT073 wild-type/Δ*pasTI* (left) and *E. coli* K-12 MG1655 wild-type/Δ*ratAB* (right) over time after inoculation from stationary phase into fresh medium (see Materials and Methods). In contrast to Figure 7a, the bacteria do not carry the empty vector pNDM220 of the complementation constructs used in Figure 7c, but this does not make a difference for *E. coli* CFT073 (compare the left panels to Figure 7a). (d) The same experiment as described in Figure 7a and (a) was performed with *E. coli* K-12 MG1655 wild-type/Δ*ratAB* carrying the pNDM220 plasmid. Note the difference in H_2O_2 sensitivity of the Δ*ratAB* mutant in panels (a) and (b) that precluded conclusive complementation experiments for this phenotype with *E. coli* K-12 MG1655 strains. (e) The fraction of cells surviving hydrogen peroxide (H_2O_2) treatment 2 hr after inoculation was determined for cultures of *E. coli* K-12 MG1655 Δ*ratAB* with and without pretreatment with the antioxidant vitamin C (ascorbate). All data points in (c-e) represent the mean of results from at least three independent experiments, and error bars indicate standard deviations. (f) The colony sizes of *E. coli* K-12 MG1655 strains harboring complementation plasmids encoding the *pasT* homolog *cc1736* from *C. crescentus* or human *coq10* under *Plac* control were analyzed on LB agar plates supplemented with 1% D-glucose (repressing expression of complementation constructs) or 1 mM IPTG (inducing expression of complementation plasmids).

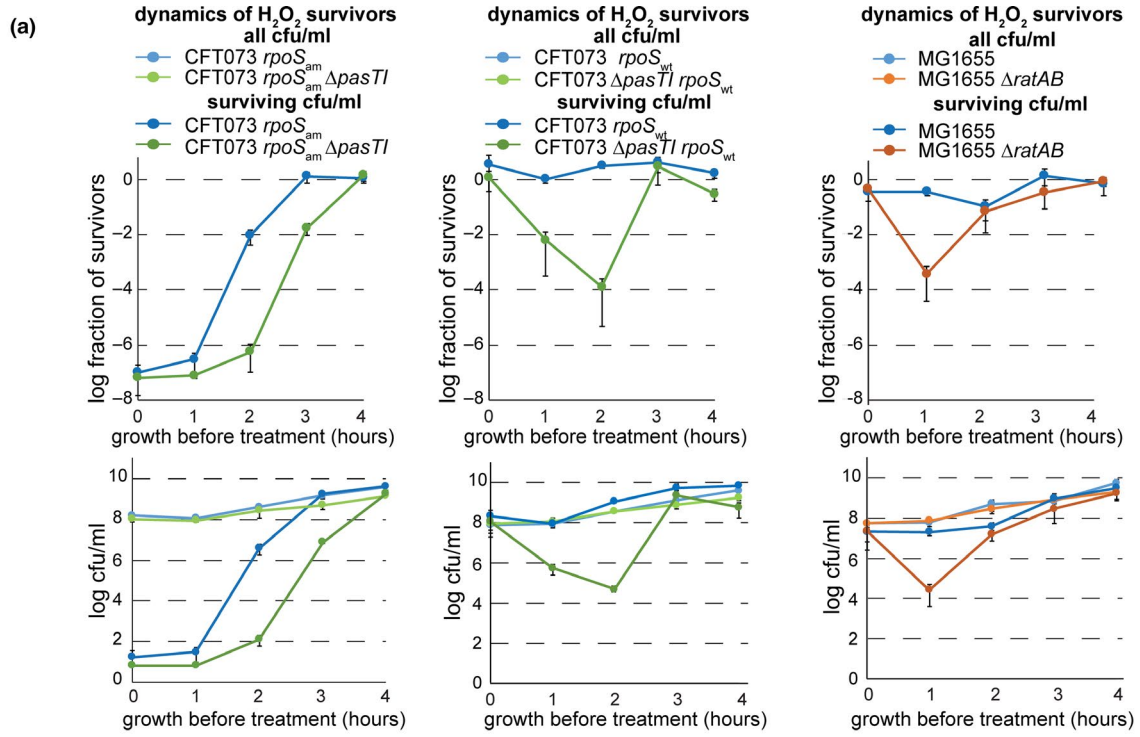
(a)
dynamics of H_2O_2 survivors
all cfu/ml
CFT073 $rpoS_{am}$
CFT073 $rpoS_{am}$ Δ*pasTI*
surviving cfu/ml
CFT073 $rpoS_{am}$
CFT073 $rpoS_{am}$ Δ*pasTI*
log fraction of survivors
growth before treatment (hours)
log cfu/ml
dynamics of H_2O_2 survivors
all cfu/ml
CFT073 $rpoS_{wt}$
CFT073 Δ*pasTI* $rpoS_{wt}$
surviving cfu/ml
CFT073 $rpoS_{wt}$
CFT073 Δ*pasTI* $rpoS_{wt}$
dynamics of H_2O_2 survivors
all cfu/ml
MG1655
MG1655 Δ*ratAB*
surviving cfu/ml
MG1655
MG1655 Δ*ratAB*

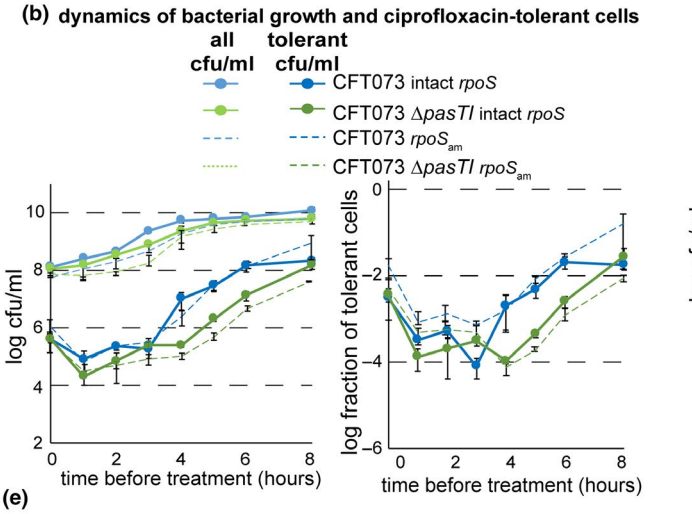
(b) dynamics of bacterial growth and ciprofloxacin-tolerant cells
all cfu/ml
tolerant cfu/ml
CFT073 intact *rpoS*
CFT073 Δ*pasTI* intact *rpoS*
CFT073 $rpoS_{am}$
CFT073 Δ*pasTI* $rpoS_{am}$
log cfu/ml
log fraction of tolerant cells
time before treatment (hours)

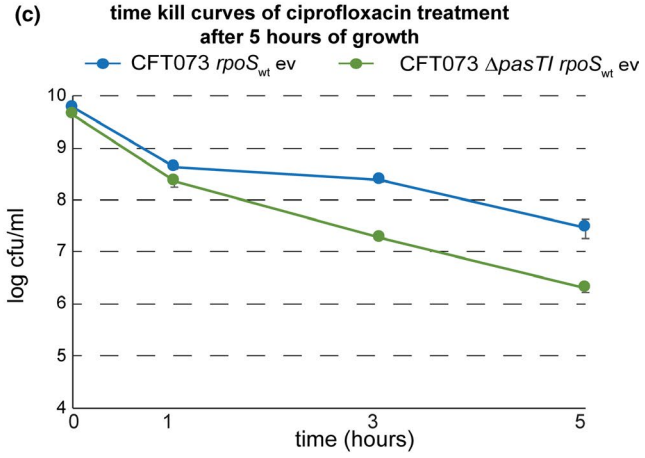
(c) time kill curves of ciprofloxacin treatment after 5 hours of growth
CFT073 $rpoS_{wt}$ ev
CFT073 Δ*pasTI* $rpoS_{wt}$ ev
log cfu/ml
time (hours)

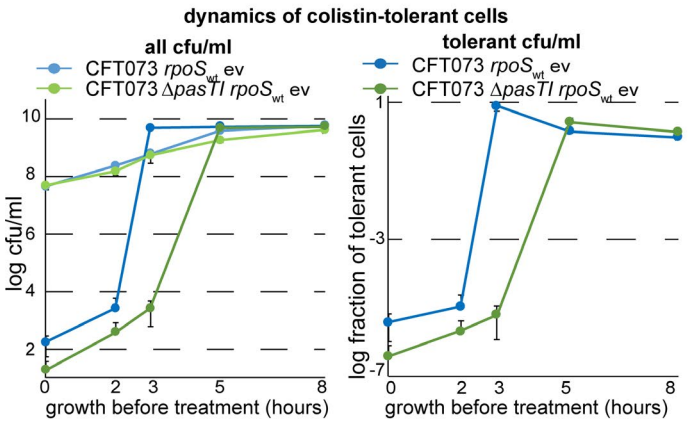
(e)
dynamics of colistin-tolerant cells
all cfu/ml
CFT073 $rpoS_{wt}$ ev
CFT073 Δ*pasTI* $rpoS_{wt}$ ev
tolerant cfu/ml
CFT073 $rpoS_{wt}$ ev
CFT073 Δ*pasTI* $rpoS_{wt}$ ev
log cfu/ml
log fraction of tolerant cells
growth before treatment (hours)

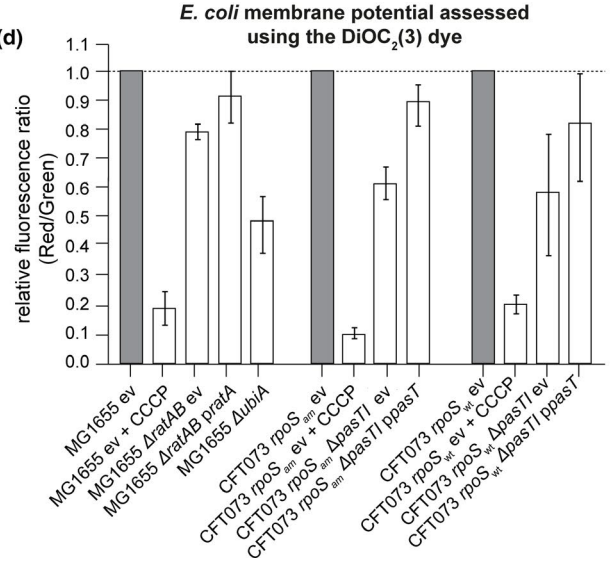
(d)
E. coli membrane potential assessed using the $DiOC_2(3)$ dye
relative fluorescence ratio (Red/Green)
MG1655 ev
MG1655 ev + CCCP
MG1655 Δ*ratAB* ev
MG1655 Δ*ratAB pratA*
MG1655 Δ*ubiA*
CFT073 $rpoS_{am}$ ev
CFT073 $rpoS_{am}$ ev + CCCP
CFT073 $rpoS_{am}$ Δ*pasTI* ev
CFT073 $rpoS_{am}$ Δ*pasTI* ppasT
CFT073 $rpoS_{wt}$ ev
CFT073 $rpoS_{wt}$ ev + CCCP
CFT073 $rpoS_{wt}$ Δ*pasTI* ev
CFT073 $rpoS_{wt}$ Δ*pasTI* ppasT

FIGURE A7 The presence of *rpoS*$_{am}$ or *rpoS*$_{wt}$ alleles in *E. coli* CFT073 Δ*pasTI* does not affect any phenotype except the dynamics of H_2O_2 survival. (a) Bacterial growth (colony-forming units (cfu)/ml) and dynamics of cells surviving hydrogen peroxide (H_2O_2) treatment were determined for cultures of *E. coli* CFT073 wild-type/Δ*pasTI* with intact *rpoS* (middle panel) in comparison with the *E. coli* CFT073 strains with the *rpoS*$_{am}$ loss-of-function allele (left panel) and the *E. coli* K-12 MG1655 strains (right panel). The left and right panels are copied from Figure A6b to enable a direct comparison. (b, c) The dynamics of ciprofloxacin tolerance throughout the growth phases of *E. coli* CFT073 and its Δ*pasTI* mutant were determined for a variant carrying an intact *rpoS* allele just like it had been done originally with the variant carrying inactive *rpoS*$_{am}$ (B; compare Figure 2a). Time–kill curves of ciprofloxacin treatment 5 hr after inoculation (c) show biphasic killing kinetics, revealing that the difference in survival at this time point is due to different levels of persister cells. (d) The membrane potential of *E. coli* CFT073 *rpoS*$_{wt}$ and its Δ*pasTI* mutant was assessed using the fluorescent indicator dye DiOC2(3) just as shown for the *rpoSam* variants in Figure 4b. All data points represent the mean of results from at least three independent experiments, and error bars indicate standard deviations. (e) Dynamics of colistin tolerance throughout the growth phases of *E. coli* CFT073, and its Δ*pasTI* mutant were determined for a variant carrying an intact *rpoS*$_{wt}$ allele as done originally for the variant carrying inactive *rpoS*am (Figure A2b).